Synthesis and Analysis of Fulleroid-Like Deployable Archimedean Mechanisms Based on an Overconstrained Eight-bar Linkage

Haohua Xiu[1], Kunyang Wang[2], Tao Xu[1], Guowu Wei[3,*], Lei Ren[2,*]

Abstract

This paper presents a novel intuitive synthesis approach for constructing Fulleroid-like Archimedean DPMs based on a Sarrus-like overconstrained spatial eight-bar linkage. Firstly, structure and the associated foundations of the eight-bar linkage are presented and characterized. Then, by integrating the eight-bar linkage into the Archimedean polyhedron bases, synthesis of a group of Fulleroid-like Archimedean DPMs is implemented; demonstrated by the design and construction of a Fulleroid-like deployable cuboctahedral mechanism and a Fulleroid-like deployable truncated tetrahedral mechanism. Subsequently, the mobility of these Fulleroid-like DPMs is verified through formulating the constraint matrices with Kirchhoff's circulation law and the associate constraint graphs. Further, kinematics of proposed polyhedral mechanisms is derived with numerical simulations, leading to the motion characterization of the eight-bar linkage and the group of Fulleroid-like deployable Archimedean mechanisms.

Keywords: Deployable Mechanism, polyhedral mechanism, overconstrained mechanism, Archimedean mechanisms, eight-bar linkage, synthesis

1. Introduction

Deployable polyhedral mechanisms (DPMs), are deployable mechanisms [1, 2] that are synthesized and constructed by integrating kinematic chains into the faces, edges and vertices of the polyhedrons. Most of DPMs are highly overconstrained mechanisms and the research on DPMs can be traced back to the flexible polyhedron proposed by Goldbergh [3], the fordable "Jitterbug" by Fuller [4] and the enlightening work "Jitterbug transformers" by Verheyen [5, 6]. The polyhedral structures Verheyen [5] proposed are formed by integrating polygonal element pairs in two-layers; it can also be derived as a special "Double Jitterbug" where two polygons in each pair are connected by revolute joints at their common edges. In spite of the original Jitterbugs, these structures are of one degree of freedom with translation and rotation along and about a virtual axis that passes through the centres of the polygons. The structures have a pattern of mirror-symmetry because of the opposite orientation of the layers.

Historically, perhaps it was the mobile octahedron named "Heureka-polyhedron" [7], exhibited at the Heureka Exposition in Zürich, firstly sparked off research interest of polyhedral mechanisms from researchers in the fields of mechanical and structural engineering, architecture and robotics. The Heureka-polyhedron was obtained from Buckminster Fuller's Jitterbug

*Corresponding authors

Email addresses: xiu_michaelcool@sina.com (Haohua Xiu), kunyang.wang@manchester.ac.uk (Kunyang Wang), xutao@jlu.edu.cn (Tao Xu), g.wei@salford.ac.uk (Guowu Wei), lei.ren@manchester.ac.uk (Lei Ren)

[1]School of Mechanical and Aerospace Engineering, Jilin University, Changchun 130000, China

[2]School of Mechanical, Aerospace and Civil Engineering, The University of Manchester, Manchester M13 9PL, United Kingdom

[3]School of Computing, Science and Engineering, University of Salford,Salford M5 4WT, United Kingdom

[4] by replacing its twelve spherical joints in the links with 2-DoF joints. The motion of the Jitterbug converting a regular octahedron via a regular icosahedron into a cuboctahedron is shown to be constrained for the Heureka-polyhedron.

After the work by Fuller, Verleyen and the Heureka-polyhedron, more research on expendable/deployable polyhedral mechanisms has been continuously presented, and among these the most notable contributions come from Wohlhart, whose work stated from the presentations of the "Turning Tower"[8]; then the spheroidal linkages [9], i.e. the "Breathing Ball", the "Spheriod", the "Star-cube" and the "Fulleroid" synthesized based on folding cotoid using the Heureka Octahedron as a basic module; the Röschel polyhedral [10, 11] linkages; the deformable cages [12] constructed by implanting a couple pairs of laminas interconnected by a set of double rotary joints into the regular ploy hedra and semi-regular polyhedral; the regular polyhedral linkages [13] generated by implanting link groups into the faces of regular polyhedrons and by interconnecting them with appropriated double gussets and multiple gussets; and the irregular polyhedral linkages [14] achieved by implanting appropriate link groups, each of which consists of a central body in the same form as the polyhedral face, into the faces of irregular polyhedra and connecting the link groups by multiple revolute whose axes intersect at the corner points of the irregular polyhedron and whose number equals the number of faces which meet at the corner points.

Another interesting work was the "Hoberman Switch Pitch", a toy that was brought to be marked by Hoberman based on his patent "geared expanding structures" [15]. The switch-pitch is also publicly called colour-changing ball; throw it into the air, the double-coloured leaves around the ball magically flip and change the colour of the ball. In addition, by embedding articulated facet linkage into polyhedrons, Gosselin et al. [16, 17, 18] proposed the RAFs, i.e. polyhedra with articulated faces. By using prismatic joints, Agrawal et al. [19] presented expanding polyhedra that can preserve their shapes. By inserting Bricard 8R- and 10R- linkages into the edges of polyhedrons, Wand and Kong [20] proposed multi-mode deployable polyhedral mechanisms. By using parallelogram linkage, Li et al. [21] constructed reconfigurable DPMs. Further, for investigating the behaviour of virus, Kovcs et al. [22] proposed a class of DPMs which were constructed by implanting prismatic faces that were connected by hinged plates along the edges of the base polyhedra. Moreover, Wei and Dai [23, 24, 25, 26, 27, 28] found that by integrating the fundamental PRRP chains, a two-ford symmetric spatial eight-bar linkage, and a one-fold symmetric eight-bar linkage into the faces, edges and vertices of the polyhedra, including the regular and semi-regular polyhedra, deployable polyhedral mechanisms with radially reciprocating motions could be formed. Furthermore, mechanical network and the associated constraint graph, and group theory [24, 29, 30] were introduced to the mobility analysis of DPMs which provides effective tools for the investigation of DPMs. Mobility and kinematic of these deployable polyhedral mechanisms, which possess cubic symmetry, can also be effectively investigated using symmetry-adapted mobility rule [31, 32, 33] .

In the above deployable polyhedral mechanisms, the Fulleroid-like mechanisms have attracted special interest from Wohlhart [13, 34] and Röschel[11, 10], with the synthesis, dynamics and self-motions having been addressed. And by using a novel Sarrus-like overconstrained eight-bar linkage, a systematic and intuitive approach has been proposed for constructing Fulleroid-like deployable Platonic mechanisms [35].

In this paper, based on the approach proposed in [35], synthesis and constructions of a group of Fulleroid-like Archimedean DPMs are generalized and presented. Structure and related formulations of an overconstrained eight-bar linkage is briefed, and by taking two typical Archimedean polyhedrons as examples, synthesis of the Archimedean DPMs is illustrated and presented. Further, mobility of the proposed mechanisms is formulated, followed by kinematic analysis and simulations of the eight-bar linkage and the proposed Fulleroid-like deployable Archimedean mechanisms.

2. A Sarrus-like Overconstrained Spatial Eight-bar Linkage

This section briefly introduces the structure of a Sarrus-like overconstrained linkage that is proposed in our previous work [35]. Mechanical structure is firstly presented, then its structure equation is developed providing kinematic background for further analysis.

2.1. Structure and Geometry of the Linkage

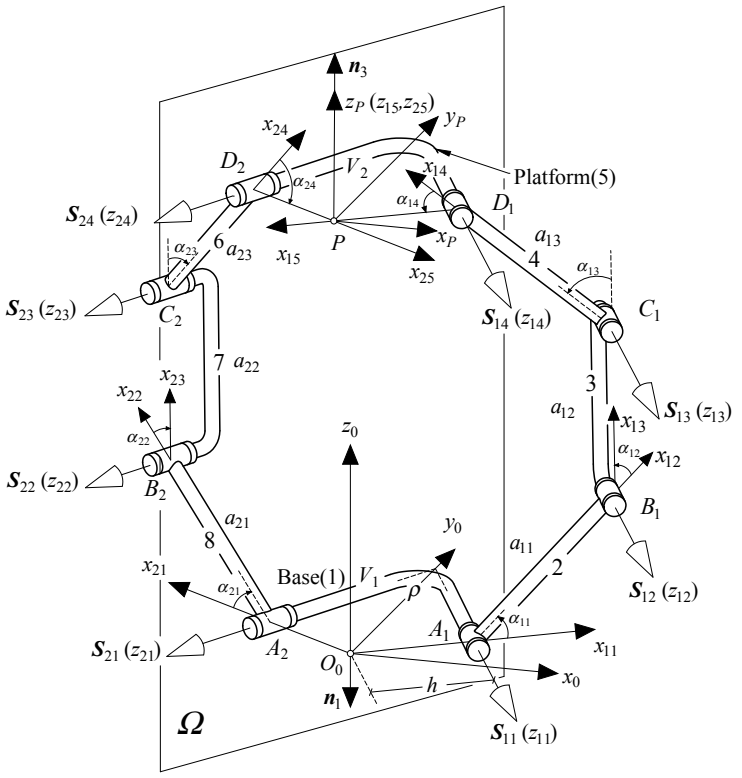

Figure 1: A Sarrus-like eight-bar linkage and its geometry.

Figure 1 illustrates the structure and the geometry of the Sarrus-like spatial eight-bar linkage. In the linkage, there are two identical isosceles V-shaped links, i.e., links V_1, V_2, one as a base (link 1 denoted as V_1) and the other one as a moving platform (link 5 denoted as V_2), each of them has revolute joints at both ends, which are joints A_1, A_2, and D_1 and D_2. Joints A_1, B_1, C_1 and D_1 are parallel to each other, and so are joints A_2, B_2, C_2 and D_2. Joints A_1, B_1, C_1 and D_1 are connected by link 2, link 3 and link 4; and similarly joints A_2, B_2, C_2 and D_2 are connected by links 6, 7 and 8. All the non-V-shaped links are of the same length. As shown in Fig. 1, the angles between the joint axes of both of the V-shaped links are ρ. This linkage is a plane symmetric with respect to plane Ω which is defined by bisectors of angles ρ of the V-shaped base and the V-shaped platform.

Regarding this eight-bar linkage as a "twined-branch" parallel kinematic mechanism with each branch starting from one side of link V_1 and ending at the same side of link V_2, one can readily find that this eight-bar mechanism bears a resemblance to the Sarrus mechanism [36]. By contrast with the Sarrus mechanism, each branch of the linkage has an extra R joint and an extra link; and this is an overconstrained mechanism like the Sarrus linkage.

2.2. Loop Equations of the Eight-bar Linkage

Structure equation of the eight-bar linkage is formulated in this section. The eight-bar linkage contains two branches with branch 1 consisting of joints A_1, B_1, C_1 and D_1, and the associated links; and branch 2 containing joints A_2, B_2, C_2 and D_2, and the coupled links. To

perform the derivation, coordinate frames are established in the linkage as illustrated in Fig.1. An inertial coordinate frame F_0-$\{x_0, y_0, z_0\}$ is established on the base (link V_1) with its origin located at point O_0, y_0-axis collinear with the bisector and z_0-axis normal to the plane formed by the axes of joints A_1 and A_2. In addition, by following the D-H convention, local coordinate frame F_{mn}-$\{x_{mn}, y_{mn}, z_{mn}\}$ are attached to the joints with the z_{mn}-axis locating along the axis of the mnth joints and the x_{mn}-axis along the common perpendicular of the $z_{m(n-1)}$-axis and z_{mn}-axis; where the first subscript m with m =1 and 2 denotes the two branches, and the second subscript n with n =1, 2, 3 and 4 stands for the joint number in the two branches. For frame F_{11}-$\{x_{11}, y_{11}, z_{11}\}$, the x_{11}-axis is perpendicular to the axis of joint A_1, and for F_{21}-$\{x_{21}, y_{21}, z_{21}\}$, the x_{21}-axis is perpendicular to the axis of joint B_1. In addition, a coordinate system F_P-$\{x_p, y_p, z_p\}$ is fixed on the moving platform (link V_2) with the y_p-axis lying on the bisector of link V_2 and the z_p-axis normal to the plane formed by axes of joints D_1-axis and D_2. In the linkage, the link length for a_{mn} are all a and the joint angles are denoted as α_{mn}, twist angles that are either 0 or $\pi/2$ are denoted as τ_{mn}. In addition, the distances from points A_1 and A_2 to point O_0 are both h. Using the about coordinate frames, the D-H parameters of the linkage can be identified and obtained.

Following the D-H parameters defined above, in the two open branches matrices ${}^{\mathbf{G}}\mathbf{T}_1$ and ${}^{\mathbf{G}}\mathbf{T}_2$ that respectively represent the transformations from frames F_{11} and F_{21} of branches 1 and 2 to the reference frame F_0 are given as ${}^{\mathbf{G}}\mathbf{T}_1 = \left[z_0\left(\frac{\rho}{2}\right), 0\right]\left[x_0\left(\frac{\pi}{2}\right), h\right]$, and ${}^{\mathbf{G}}\mathbf{T}_2 = \left[z_0\left(\pi - \frac{\rho}{2}\right), 0\right]\left[x_0\left(-\frac{\pi}{2}\right), h\right]$; and the homogeneous transformation matrices $\mathbf{T}_{mn}$ between two adjacent coordinate frames are expressed as

$$\mathbf{T}_{mn} = [z_{mn}(\alpha_{mn}, d_{mn})][x_{mn}(\tau_{mn}, a_{mn})] \tag{1}$$

Further, given the transformations from frames F_{14} and F_{24} to frame F_P with $\mathbf{H_1} = \left[z_{15}\left(\pi - \frac{\rho}{2}\right), 0\right][x_{15}(0,0)]$ and $\mathbf{H_2} = \left[z_{25}\left(\frac{\rho}{2}\right), 0\right][x_{25}(0,0)]$, respectively, the structure equation for each open branch can be formed as follows.

For branch 1 it has

$$\mathbf{D}_{\text{branch 1}} = {}^{\mathbf{G}}\mathbf{T}_1\mathbf{T}_{11}\mathbf{T}_{12}\mathbf{T}_{13}\mathbf{T}_{14}\mathbf{H}_1 \tag{2}$$

and for branch 2 it has

$$\mathbf{D}_{\text{branch 2}} = {}^{\mathbf{G}}\mathbf{T}_2\mathbf{T}_{21}\mathbf{T}_{22}\mathbf{T}_{23}\mathbf{T}_{24}\mathbf{H}_2 \tag{3}$$

Hence, by equating the above two equations, structure equation for the eight-bar linkage is

$${}^{\mathbf{G}}\mathbf{T}_1\mathbf{T}_{11}\mathbf{T}_{12}\mathbf{T}_{13}\mathbf{T}_{14}\mathbf{H}_1 = {}^{\mathbf{G}}\mathbf{T}_2\mathbf{T}_{21}\mathbf{T}_{22}\mathbf{T}_{23}\mathbf{T}_{24}\mathbf{H}_2 \tag{4}$$

2.3. Mobility of the Eight-bar Linkage

As aforementioned, the proposed eight-bar linkage is an overconstrained mechanism like the Sarrus linkage. As formulated in [35] with screw-theory, the motion-screw system $\mathbb{S}_f$ of the moving platform (link V_2) is of three-system [37] as

$$\mathbb{S}_f = \begin{cases} \boldsymbol{S}_{f1} = \begin{bmatrix} 0 & 0 & 0 & 1 & 0 & 0 \end{bmatrix}^{\mathrm{T}} \\ \boldsymbol{S}_{f2} = \begin{bmatrix} 0 & 0 & 0 & 0 & 1 & 0 \end{bmatrix}^{\mathrm{T}} \\ \boldsymbol{S}_{f3} = \begin{bmatrix} 0 & 0 & 0 & 0 & 0 & 1 \end{bmatrix}^{\mathrm{T}} \end{cases} \tag{5}$$

which is the span of motion-screw system $\mathbb{S}_i$ of each ranch.

Equation (5) implies that the moving platform of the spatial eight-bar linkage has 3-DOF with link V_1 being a fixed base, which are translations along the x_0-axis, y_0-axis and z_0-axis; and therefore mobility of the linkage is three. However, corresponding to the Chebychev-Grübler-

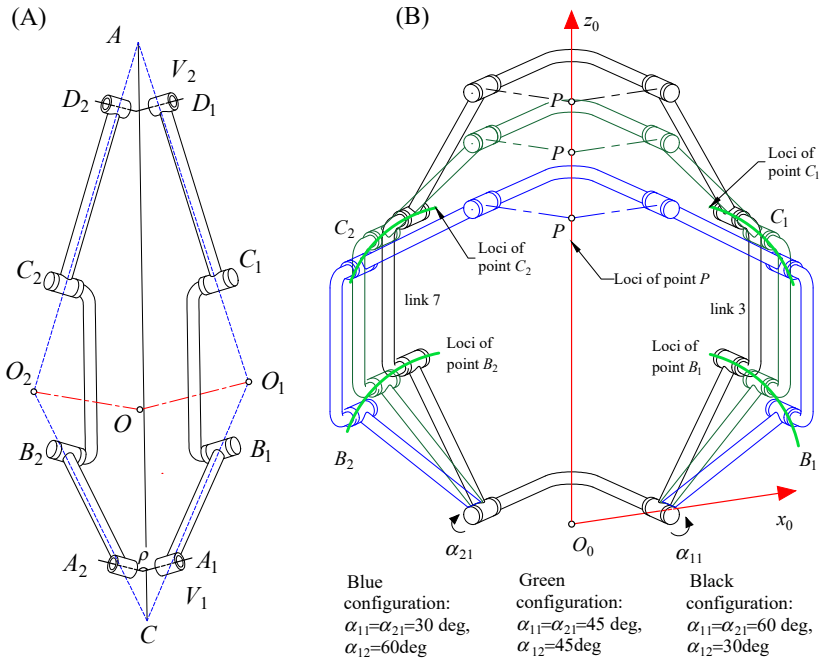

Figure 2: Loci of B_1, B_2, C_1, C_2 and P in the condition of giving symmetric inputs $\alpha_{11} = \alpha_{21}$.

Kutzbach's equation [37], mobility of this linkage is two. Thus, the proposed spatial eight-bar linkage is overconstrained.

2.4. Features of the Eight-bar Linkage

Considering the similarity of the proposed eight-bar linkage with the Sarrus linkage, it is supposed that by given proper inputs, the moving platform (link V_2) will implement straight-line motion on the symmetric plane Ω. Since this is a 3-DOF linkage, three inputs must be provided and to achieve the straight-line motion of the moving platform, these three inputs must satisfy certain conditions. In this paper, it is found that there are two cases that can lead to the desired motion with different conditions.

Figure 2(A) shows the first case in which three inputs are α_{11}, α_{21} and α_{12} with the two grounded inputs α_{11}, α_{21} satisfying $\alpha_{11} = \alpha_{21}$. The initial configuration of eight-bar linkage is set as: in branch 1, links 3 and 7 are parallel to each other, the angle between link 2 and link 3 is 150 deg and the angle between link 3 and link 4 is 150 deg; in branch 2, the angle between link 6 and link 7 is 150 deg and the angle between link 7 and link 8 is 150 deg. In this initial configuration, there are four intersection points derived from the extensions of links 2, 4, 6 and link 8 (blue dash-line) symbolized as points A, C, O_1 and O_2. Perpendicular lines (red dash-line) respectively perpendicular to planes ACO_1 and ACO_2 passing through O_1 and O_2 intersect at point O. In this case, the moving platform implements reciprocating straight-line motion relative to point O, which is regarded as virtual central point of the eight-bar linkage. Like Sarrus linkage, the locus of the platform can be presented by the point P, as shown in Fig. 2(B), is a straight line. In the meantime, link 3 and link 7 are able to achieve spatial motion (symmetrical about plane ACO) with their orientations unchanged .

The other case is indicated in Fig. 3, unlike the first case, it demands that links 3 and 7 carry out skew-symmetric screw motion. In order to perform such motion, the geometric condition to be satisfied is $\alpha_{11} = \alpha_{24}$ or $\alpha_{14} = \alpha_{21}$ which is derived in details as follows.

Referring to Fig. 3(A), the two perpendicular lines OO_1 and OO_2 of the planes ACO_1 and ACO_2 intersect at the virtual centre point O. The normals $\boldsymbol{n}_2$ and $\boldsymbol{n}_4$ are respectively outwards along lines OO_1 and OO_2. Assume that the mobile platform executes reciprocating straight-line motion, considering that the linkage is symmetric about the plane ACO, it implies that point P

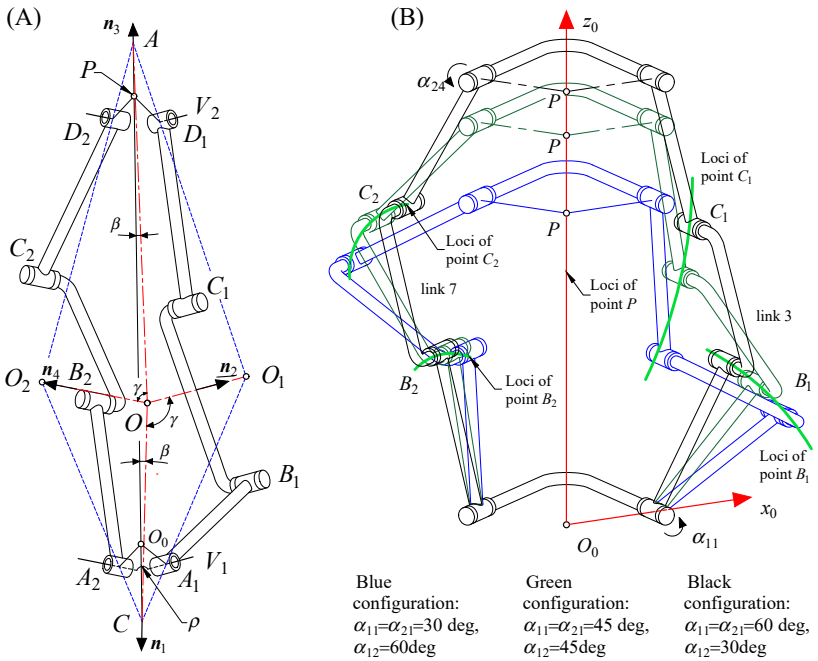

Figure 3: Loci of B_1, B_2, C_1, C_2 and P in the condition of giving skew-symmetric inputs $\alpha_{11} = \alpha_{24}$ or $\alpha_{14} = \alpha_{21}$.

must be placed on Ω such that the x-coordinate of P is 0. Given the coordinates from $\mathbf{D}_{\text{branch 1}}$ and $\mathbf{D}_{\text{branch 2}}$ in Eqns. (2) and (3) as x_{P_1} and x_{P_2}, respectively, it has

$$x_{P_1} = Xa + Yh = 0 \tag{6}$$

and

$$x_{P_2} = X'a + Y'h = 0 \tag{7}$$

with

$$X = \cos\left(\frac{\rho}{2}\right)\left[\cos\alpha_{11} + \cos\left(\alpha_{11}+\alpha_{12}\right) + \cos\left(\alpha_{11}+\alpha_{12}+\alpha_{13}\right)\right]$$

$$Y = \cos\left(\frac{\rho}{2}\right)\left[1 + \cos\left(\alpha_{11}+\alpha_{12}+\alpha_{13}+\alpha_{14}\right)\right]$$

$$X' = \cos\left(\frac{\rho}{2}\right)\left[\cos\alpha_{21} + \cos\left(\alpha_{21}+\alpha_{22}\right) + \cos\left(\alpha_{21}+\alpha_{22}+\alpha_{23}\right)\right]$$

$$Y' = \cos\left(\frac{\rho}{2}\right)\left[1 + \cos\left(\alpha_{21}+\alpha_{22}+\alpha_{23}+\alpha_{24}\right)\right]$$

Since a, h are constant as structure parameters, and ρ is less than 180 deg, Eqns. (6) and (7) indicate that the values of X, Y, X' and Y' have to be zero, which result in the following relations

$$\begin{cases} \cos\alpha_{11} + \cos\left(\alpha_{11}+\alpha_{12}\right) + \cos\left(\alpha_{11}+\alpha_{12}+\alpha_{13}\right) = 0 \\ \alpha_{11}+\alpha_{12}+\alpha_{13}+\alpha_{14} = \pi \end{cases} \tag{8}$$

and

$$\begin{cases} \cos\alpha_{21} + \cos\left(\alpha_{21}+\alpha_{22}\right) + \cos\left(\alpha_{21}+\alpha_{22}+\alpha_{23}\right) = 0 \\ \alpha_{21}+\alpha_{22}+\alpha_{23}+\alpha_{24} = \pi \end{cases} \tag{9}$$

Using the relations in Eqns. (8) and (9), the position vector for point P in the moving platform can be expressed in branch 1 and branch 2, respectively as

$$\boldsymbol{p}_1 = \begin{bmatrix} x_p \\ y_p \\ z_p \end{bmatrix} = \begin{bmatrix} 0 \\ 0 \\ a\left[\sin\alpha_{11} + \sin\left(\alpha_{11}+\alpha_{12}\right) + \sin\left(\alpha_{11}+\alpha_{12}+\alpha_{13}\right)\right] \end{bmatrix} \tag{10}$$

and

$$\boldsymbol{p}_2 = \begin{bmatrix} x_p \\ y_p \\ z_p \end{bmatrix} = \begin{bmatrix} 0 \\ 0 \\ a\left[\sin\alpha_{21} + \sin\left(\alpha_{21}+\alpha_{22}\right) + \sin\left(\alpha_{21}+\alpha_{22}+\alpha_{23}\right)\right] \end{bmatrix} \tag{11}$$

Both Eqns. (10) and (11) imply that the platform has a restricted movement which only a translation along the z-axis direction, i.e., the platform implements a strict straight-line motion.

Further, in Fig. 3 assuming that the V-shaped link 1 is no longer treated as a fixed base, it is found that if the given inputs meet the condition $\alpha_{11} = \alpha_{24}$, $\alpha_{12} = \alpha_{23}$ and $\alpha_{13} = \alpha_{22}$, the links 3 and 7 will execute screw motion around OO_1 and OO_2 respectively while the links 1 and 5 are able to carry out radially reciprocating movement along CO and AO. In this case, the angles between OO_1 and CO, OO_2 and OA are the same, declared as γ. From this configuration, there exists

$$\boldsymbol{n}_1^T \boldsymbol{n}_2 = \boldsymbol{n}_3^T \boldsymbol{n}_4 \tag{12}$$

where $\boldsymbol{n}_1$ and $\boldsymbol{n}_3$ can be derived from Figs. 1 and 3 as

$$\boldsymbol{n}_1 = \begin{bmatrix} 1 & 0 & 0 \\ 0 & \cos(-\beta) & -\sin(-\beta) \\ 0 & \sin(-\beta) & \cos(-\beta) \end{bmatrix} \begin{bmatrix} 0 \\ 0 \\ -1 \end{bmatrix} = \begin{bmatrix} 0 \\ -\sin\beta \\ -\cos\beta \end{bmatrix} \tag{13}$$

and

$$\boldsymbol{n}_3 = \begin{bmatrix} 1 & 0 & 0 \\ 0 & \cos\beta & -\sin\beta \\ 0 & \sin\beta & \cos\beta \end{bmatrix} \begin{bmatrix} 0 \\ 0 \\ 1 \end{bmatrix} = \begin{bmatrix} 0 \\ -\sin\beta \\ \cos\beta \end{bmatrix} \tag{14}$$

The normals $\boldsymbol{n}_2$ and $\boldsymbol{n}_4$ can be respectively extracted from the homogeneous coordinates of joints B_1 and B_2 as

$$\boldsymbol{n}_2 = \begin{bmatrix} \sin\left(\dfrac{\rho}{2}\right) \\ -\cos\left(\dfrac{\rho}{2}\right) \\ 0 \end{bmatrix} \tag{15}$$

and

$$\boldsymbol{n}_4 = \begin{bmatrix} -\sin\left(\dfrac{\rho}{2}\right) \\ -\cos\left(\dfrac{\rho}{2}\right) \\ 0 \end{bmatrix} \tag{16}$$

Substituting Eqns. (13) to (16) into Eqn. (12) leads to the results that $\boldsymbol{n}_1^T \boldsymbol{n}_2 = \boldsymbol{n}_3^T \boldsymbol{n}_4 = \sin\beta\cos\left(\rho/2\right) = \cos\gamma$, which means once the dimension of the V-shaped link of eight-bar linkage is determined, by using the above analysis, the angles γ and β are determined.

Then equating Eqns. (10) and (11), there exists

$$\begin{aligned} &\sin\alpha_{11} + \sin(\alpha_{11} + \alpha_{12}) + \sin(\alpha_{11} + \alpha_{12} + \alpha_{13}) = \\ &\sin\alpha_{21} + \sin(\alpha_{21} + \alpha_{22}) + \sin(\alpha_{21} + \alpha_{22} + \alpha_{23}) \end{aligned} \tag{17}$$

Substituting Eqns. (8) and (9) into Eqn. (17), it yields

$$\begin{aligned} &\sin\alpha_{11} + \sin(\alpha_{13} + \alpha_{14}) + \sin\alpha_{14} = \\ &\sin\alpha_{21} + \sin(\alpha_{21} + \alpha_{22}) + \sin\alpha_{24} \end{aligned} \tag{18}$$

Giving the condition that $\alpha_{11} = \alpha_{24}$, Eqn. (18) can be further simplified as

$$\sin(\alpha_{13} + \alpha_{14}) + \sin\alpha_{14} = \sin\alpha_{21} + \sin(\alpha_{21} + \alpha_{22}) \tag{19}$$

Referring to Fig. 3, assuming that $\alpha_{21} = \alpha_{14}$, we have

$$\sin(\alpha_{13} + \alpha_{14}) = \sin(\alpha_{21} + \alpha_{22}) \tag{20}$$

which means the equation $\alpha_{11} + \alpha_{12} = \alpha_{23} + \alpha_{24}$ exists and hence we have $\alpha_{12} = \alpha_{23}$ and $\alpha_{13} = \alpha_{22}$.

Therefore, it is evidently proved that once meet the requirements of $\alpha_{11} = \alpha_{24}$, $\alpha_{12} = \alpha_{23}$ and $\alpha_{13} = \alpha_{22}$ and given three skew-symmetric inputs, the moving platform executes an strict straight-line motion; and the four joints which belonged to link 3 and link 7 are able to perform double helix motion (shown in green lines) as illustrated in Fig. 3(B).

Based on the motion features of the proposed eight-bar linkage, it is well used for synthesizing and constructing Fulleroid-like Archimedean DPMs by properly implanting it into the group of Archimedean polyhedron bases, more details as shown in the following sections.

3. Synthesis & Construction of Fulleroid-like Archimedean DPMs

Syntheses and constructions of the Fulleroid-like Archimedean DPMs are presented in this section. It is well known that there are thirteen Archimedean polyhedrons first enumerated by Archimedes. For illustration purpose, the cuboctahedron and truncated tetrahedron are selected from the group of Archimedean polyhedrons as examples for the synthesis. A cuboctahedron, from the geometry perspective, has 6 square faces and 8 equilateral triangular faces; it has 12 identical vertices, each of which is formed by the intersection of two triangles and two squares; it also has twenty-four identical edges, each separating a triangle from a square. A truncated tetrahedron has four regular hexagonal faces, four equilateral triangular faces, twelve vertices and eighteen identical edges. The main difference between these two Archimedean solids is that in the truncated tetrahedron, a hexagonal face not only shares edges with other hexagonal faces but also shares edges with other triangular faces. By respectively inserting a batch of the proposed eight-bar linkage into the cuboctahedron base and the truncated tetrahedron base, the Fulleroid-like deployable cuboctahedral mechanism and tetrahedral truncated mechanism are synthesized and constructed in this section; and this methodology can readily be extended and generalized to the synthesis of the whole group of Archimedean polyhedra.

3.1. Synthesis & Construction of A Fulleroid-like Deployable Cuboctahedral Mechanism

The cuboctahedron is one of well-known Archimedean solids which is a semi-regular convex polyhedron composed of equilateral triangles and squares. These triangles and squares meet in identical vertices by sharing an identical edge. A cuboctahedron is illustrated in Fig. 4; it has 14 faces, with the triangular faces numbered from f_1 to f_8 and the square faces numbered from f_9 to f_{14}. The 12 vertices are labelled as A, B, C,$\cdots$, L and 24 edges denoted by e_1 throughout

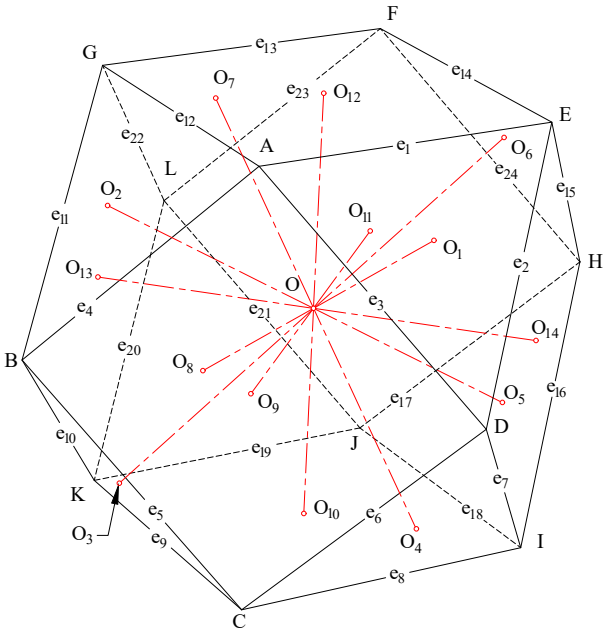

Figure 4: A regular cuboctahedron base and its geometry.

e_{24}. Points O_1, O_2, $\cdots$, O_8 and O_9, O_{10}, $\cdots$, O_{14} are the centroids of eight triangles and six squares. According to the property of a cuboctahedron, the line segments O_1O_8, O_2O_5, O_3O_6, O_4O_7, O_9O_{11}, $O_{10}O_{12}$, $O_{13}O_{14}$ are all perpendicular to the corresponding faces and intersect at point O, i.e. the centroid of the cuboctahedron. The cuboctahedron here is used as a base for synthesizing a Fulleroid-like featured deployable cuboctahedral mechanism. As shown in Fig. 4, line segments in red central lines are treated as *virtual axes* and point O is defined as the *virtual centre* of the deployable cuboctahedral mechanism to be constructed.

In the cuboctahedron base, as shown in Fig. 5(A), the first eight-bar linkage is arranged along e_3. In this implant, the axes of all revolute joints A_1, B_1, C_1 and D_1 from branch 1 are normal to face f_1. Similarly, the axes of all revolute joints from branch 2 are perpendicular to the adjacent face f_9. The joints B_1 and C_1 are not allowed to be aligned with either the bisector of $\angle$DAE which is AO_1 or the bisector of $\angle$ADE which is O_1D. It is noted that f_1 will occupy a branch from an eight-bar linkage, but the height of f_1 is lower than the length of the edge. On the face f_9, joints A_2 and B_2 are aligned with the diagonal of f_9 denoted as AO_9, joints C_2 and D_2 are collinear with another diagonal of f_9, i.e. O_9D. Referring to Fig. 4, the dihedral angle α of the cuboctahedron can be calculated as $\alpha_{\text{cub}} = \text{arcsec}\left(-\sqrt{3}\right)$. So the angle of the V-shaped link of eight-bar linkage must satisfy the condition that $\rho_{\text{cub}} = 180^\circ - \alpha_{\text{cub}}$ and lengths of the all links in the two branches have to remain the same value.

Next, the second eight-bar linkage is embedded along e_1 as illustrated in Fig. 5(B). At this time, it owns and shares link A_1B_1 with the previous linkage, which means link A_3B_3 remained unchanged such that joints C_3 and D_3 are orthogonal to f_1. The axes of joints A_4, B_4, C_4 and D_4 are normal to f_{12} which shares the same edge e_1 with face f_1. On face f_1, joint B_3 is not allowed to be aligned with AO_1 and joint C_3 is not allowed to be aligned with the bisector of $\angle$AED which is D_3O_1. On the face f_{12}, joints A_4 and B_4 lie on the diagonal AO_{12} and joints C_4 and D_4 lie on the diagonal $O_{12}E$.

After integrating the two eight-bar linkages, the very same procedure is processed and two more eight-bar linkages are mounted along edges e_{12} and e_4 (see Fig. 5(C) and (D)) until we get the first preliminary vertex around point A of the Fulleroid-like deployable cuboctahedral mechanism. Moreover, by integrating twenty more eight-bar linkages along the rest edges, a Fulleroid-like deployable cuboctahedral mechanism is generated as shown in Fig. 6. This deployable mechanism is comprised of eight equilateral triangular facet components labelled

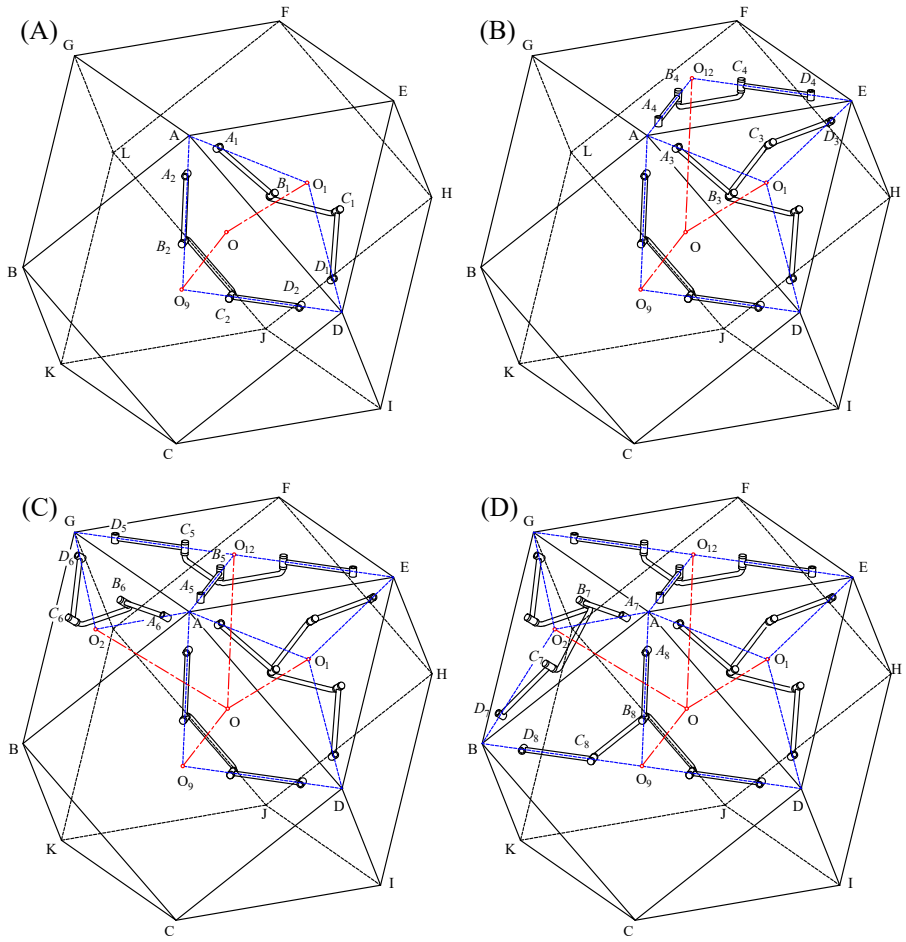

Figure 5: Synthesis of a Fulleroid-like deployable cuboctahedral mechanism.

from V_1 to V_8, six square facet components numbered from V_9 to V_{14}; each equilateral triangular component hooks up three identical links with pins through the joints, and the length of link equal to the side of the component. Similarly, each square facet component has four identical links connected with same length. All the links connected to two different facet components are identical. In addition, twelve vertex components labelled as V_A, $\cdots$, V_L are formed. Due to the property of the eight-bar linkage, given a torque on any facet component around its virtual axis, all the other components are able to carry out screw motions around the corresponding virtual axes; and all vertices are capable of accomplish reciprocating motion along their corresponding virtual axes.

Figure 6(A) shows the fully expanded configuration of the mechanism, in this configuration each part of this mechanism arrives at the distal end along the associated virtual axes; on the contrary, in Fig.6(C), the completely folded configuration, every link in this mechanism overlaps one side of a facet component. The above demonstrates how to synthesize a Fulleroid-like deployable cuboctahedral mechanism. Nevertheless, so far it has not yet confirmed whether this synthesizing method can be extended and applied to the whole group of Archimedean solids. In order to further verify the suitability for Archimedean solids, we changed the cuboctahedron base to a truncated tetrahedron base. The truncated tetrahedron is another typical Archimedean polyhedron which has a different feature from the cuboctahedron as we mentioned before: one of the two different polygonal faces is not only sharing edges with another kind of polygonal face but also with the same kind. The detailed synthesis and construction process is shown in the following section.

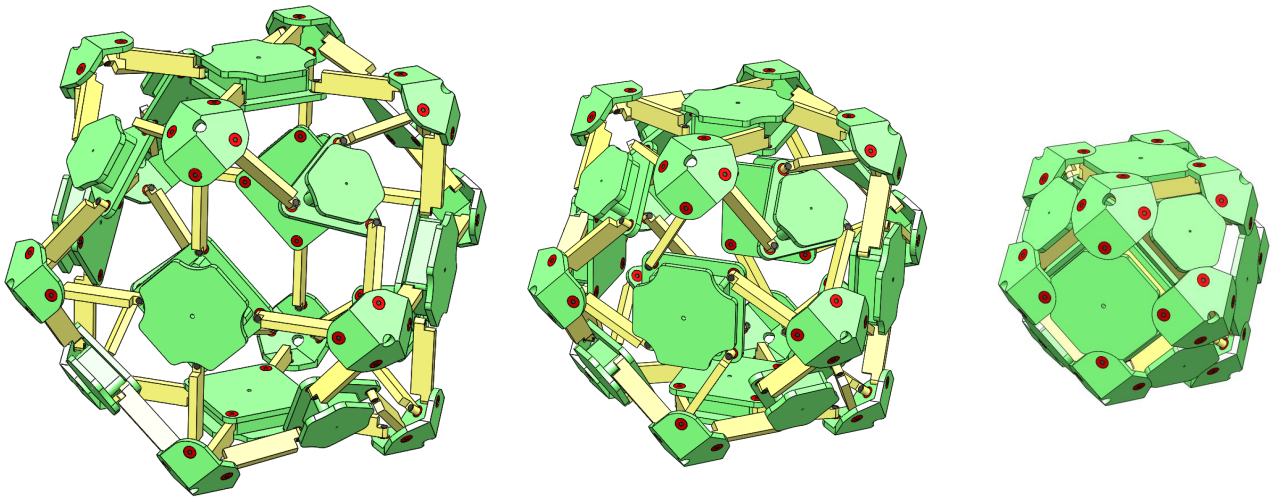

(A) completely expanded (B) intermediate configuration (C) completely folded

Figure 6: A Fulleroid-like deployable cuboctahedral mechanism in three configurations.

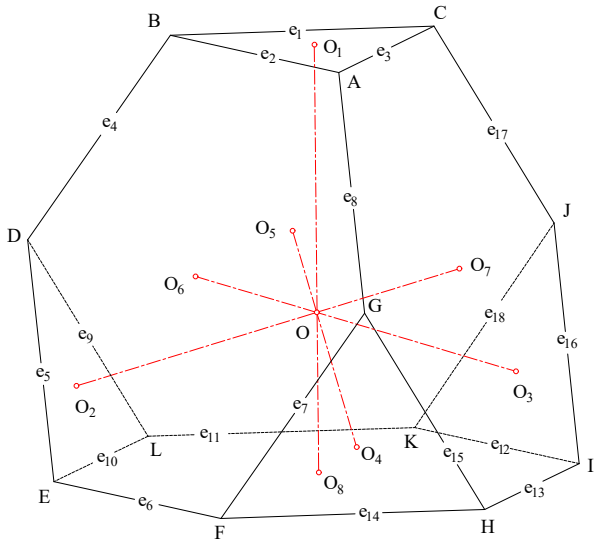

Figure 7: A regular truncated tetrahedron base and its geometry.

3.2. Synthesis & Construction of A Fulleroid-like Deployable Truncated Tetrahedral Mechanism

Fig. 7 shows a regular truncated tetrahedron, it consist of four equilateral triangular faces, numbered from f_1 to f_4, and four hexagonal faces numbered as f_5, f_6, f_7, f_8; its eighteen edges are declared as e_1 throughout e_{18}, which precisely organize twelve vertices from A throughout L. Points O_1, $\cdots$, O_4 are the centroids of the four triangular faces, and points O_5, $\cdots$, O_8 are the centroids of the four hexagonal faces so that four line segments O_1O_8, O_2O_7, O_3O_6 and O_4O_5 are all normal to the corresponding faces and cisscross at point O, the centroid of the truncated tetrahedron. This truncated tetrahedron is employed as a base for synthesizing a Fulleroid-like deployable truncated tetrahedral mechanism with O_1O_8, O_2O_7, O_3O_6 and O_4O_5 being consulted as virtual axes and point O being consulted as the virtual centre.

In the truncated tetrahedron base, as illustrated in Fig. 8(A), place the first eight-bar linkage embedded along the e_7. Make sure that all the axes of joints from branch 1 and branch 2 are respectively normal to faces f_4 and f_6. On face f_6, joints A_2, B_2 are aligned with FO_6, joints C_2 and D_2 are aligned with GO_6. With regards to f_4, joint B_1 is not able to aligned with FO_4 while C_1 can not be aligned with GO_4 since the deficient space for settling the third identical link in the case that link A_1B_1 and C_1D_1 are coincided with FO_4 and GO_4. Because of

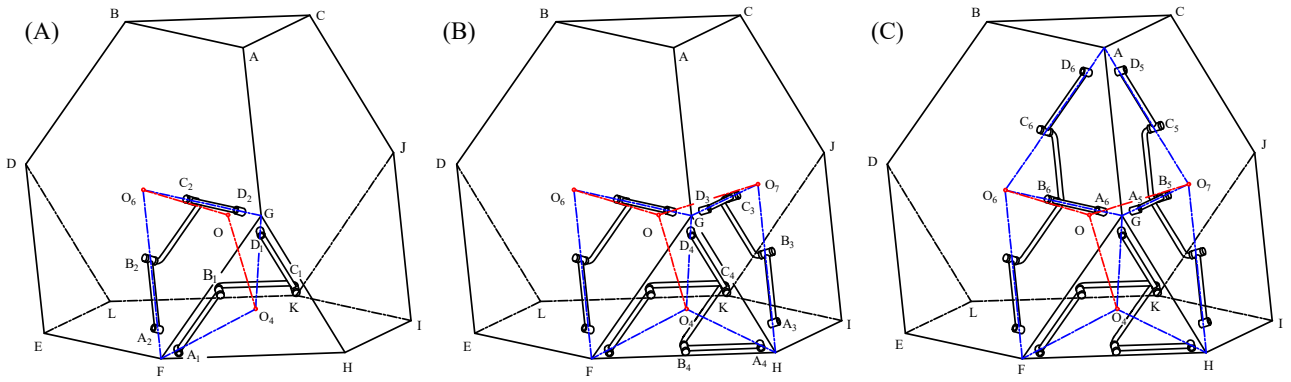

Figure 8: Synthesis of Fulleroid-like deployable truncated tetrahedral mechanism.

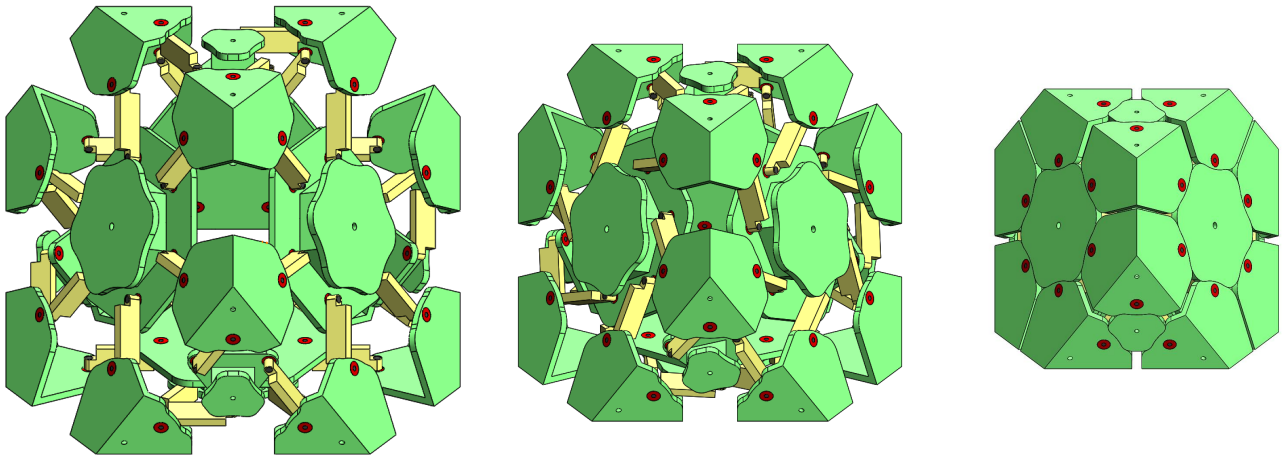

(A) completely expanded (B) intermediate configuration (C) completely folded

Figure 9: A Fulleroid-like deployable truncated tetrahedral mechanism in three configurations.

the characteristics of the truncated tetrahedron base, there are two dihedral angles which can be calculated as: the dihedral angle between triangular face and hexagonal face is $109°28''16'$, and the dihedral angle between two hexagonal faces is $70°31''44'$. In pursuance of building a Fulleroid-like mechanism by embedding the proposed eight-bar linkage into the truncated tetrahedron base, referring to the previous subsection, the angles of R-R dyads have to satisfy $\rho_{\text{trun}_1} = 70°31''44'$ when forming the vertex which holds triangular face and hexagonal face and $\rho_{\text{trun}_2} = 109°28''16'$ when building the vertex that holds two hexagonal faces.

Following the same operation, we implant the second eight-bar linkage along edge e_{15} by sharing the link C_4D_4 with the previous eight-bar linkage, that is, link C_1D_1 is on a par with link C_4D_4, as illustrated in Fig. 8(B). The axes of joints A_4, B_4, C_4 and D_4 are normal to f_4 while B_4, C_4 can not be aligned with GO_4 and LO_4, meanwhile, axes of joints A_3, B_3, C_3 and D_3 are normal to f_7 with joints A_3 and B_3 lie on HO_7, C_3 and D_3 lie on GO_7.

Further, the third integration is carried out along edge e_8 which being shared by two identical hexagonal faces f_6 and f_7. So in the third integration of eight-bar linkage, see Fig. 8(C), link A_5B_5 is shared by link D_3C_3 from the second integration of eight-bar linkage and A_6B_6 is shared by link D_2C_2 from the first integration of the eight-bar linkage. Note that in the third integration, the value of angle of V-shaped link should be $109°28''16'$.

The above gives the principal steps for integrating the proposed eight-bar linkages into a truncated tetrahedron base. One can take these three steps for synthesizing one single preliminary vertex of the Fulleroid-like deployable mechanism because each vertex is formed by three faces (two hexagonal faces and one triangular face). It is intuitive and straightforward that we only need to repeat the mentioned steps for integrating eight-bar linkages along the rest edges

and then followed by implementing a further specified goal-oriented structural processing, a Fulleroid-like deployable mechanism is created as demonstrated in Fig. 9.

The whole mechanism consists of eighteen independent loops, which loop forms eight-bar linkage with four triangular facet components named as V_1, $\cdots$, V_4, and four hexagonal facet components named as V_5, $\cdots$, V_8. The length of side of triangular component is the same as that of the hexagonal component. Each triangular component is connected with three identical links. Similarly, each hexagonal facet component is attached with six identical links. As discussed in previous sections, all link lengths equal the length of the side of facet components which means there is only one identical link exists. In the mechanism, there are twelve vertex components named V_A throughout V_L. All the facet components operate screw-motions around their associated virtual axes and all the vertex components implement radially reciprocating movements along their corresponding virtual axes.

Figure 9 shows the detailed design of a Fulleroid-like deployable truncated tetrahedral mechanism. From Fig. 9(A) that in completely expanded configuration, each vertex and facet component reaches the extreme position; and in fully folded configuration, as indicated in Fig. 9(C), links are sheltered by the facet components which means all parts reach the proximal-end positions.

3.3. Number Synthesis & Construction of Fulleroid-like Archimedean DPMs

Previous sections present the syntheses and constructions of two Fulleroid-like DPMs based on two typical Archimedean polyhedron bases through integrating the overconstrained eight-bar-linkage. Without loss of generality, this synthesizing method of can be naturally extended and generalized based on other bases from the group of Archimedean polyhedra. According to [28], semi-regular polyhedrons such as Archimedean solids have the same properties on numbers of links and joints. Thus, the number synthesis for the whole group of Fulleroid-like Archimedean DPMs is presented in this section.

By recalling the geometrical traits of the Archimedean polyhedrons with the Euler's formula for a polyhedron, the number of links and joints for each of the Archimedean mechanisms are given as

$$N_{link} = v + f + \sum_{i=1}^{f} s_i + \sum_{j=1}^{f} s_j = 3e + 2 \tag{21}$$

and

$$N_{joint} = 2\sum_{j=1}^{f} s_j = 4e \tag{22}$$

where f, v, e denote the numbers of faces, vertices, and edges in the given Archimedean solid base, satisfying $v - e + f = 2$. Hence, consider the synthesizing approach used for the construction of the aforementioned two mechanisms, based on the structure parameters of the Archimedean solids identified in Table 1, where N_{link} and N_{joint} provide the number of links and joints, and γ_1, γ_2 give the angles between the locus of vertex and the two corresponding perpendicular line of two facet components, ρ represents the angle of V-shaped link in eight-bar linkage forming the vertex. The whole group of Archimedean polyhedrons can be synthesized and transformed into Fulleroid-like DPMs. As can be seen in Table 1, some mechanisms are formed by two regular polygons such as the cuboctahedral mechanism and truncated tetrahedral mechanism, some are formed by three regular polygons such as the deployable Fulleroid-like truncated icosidodecahedral mechanism and the deployable Fulleroid-like rhombicosidodecahedral mechanism, they all synthesized and constructed based on the proposed overconstrained 8-bar linkage. Because of the special kinematic characterization and the synthesizing method,

Table 1: Numbers of links and joints of Fulleroid-like Archimedean DPMs

Deployable mechanisms	N_{link}	N_{joint}	Formed by	γ_1(deg)	γ_2(deg)	ρ(deg)
Truncated tetrahedral	56	72	Triangle-Hexagon	29.5	58.52	70.53
			Hexagon-Hexagon	58.52	58.52	109.47
Cuboctahedral	74	96	Triangle-Square	54.74	45	54.74
Truncated cube	110	144	Triangle-Octagon	18.94	47.27	54.74
			Octagon-Octagon	47.27	47.27	90
Truncated octahedra	110	144	Square-Hexagon	26.57	39.23	54.74
			Hexagon-Hexagon	39.23	39.23	70.53
Rhombicuboctahedral	146	192	Triangle-Square	24.37	30.36	35.26
			Square-Square	30.36	30.36	45
Truncated cuboctahedral	218	288	Square-Hexagon	17.75	25.56	35.26
			Square-Octagon	17.76	34.32	45
			Hexagon-Octagon	25.26	34.32	54.74
Snub cube	182	240	Triangle-Square	25.45	31.75	37.02
			Triangle-Triangle	25.45	25.45	26.77
Icosidodecahedral	182	240	Triangle-Pentagon	20.91	31.72	37.38
Truncated dodecahedral	272	360	Triangle-Decagon	11.21	33.02	37.38
			Decagon-Decagon	11.21	33.02	63.43
Truncated icosahedral	272	360	Pentagon-Hexagon	20.08	23.8	37.38
			Hexagon-Hexagon	23.8	23.8	41.81
Rhombicosidodecahedral	362	480	Triangle-Square	14.98	18.46	20.91
			Square-Pentagon	18.46	22.39	31.72
Truncated icosidodecahedral	542	720	Square-Hexagon	10.72	15.25	20.91
			Square-Decagon	10.72	25.18	31.72
			Hexagon-Decagon	15.25	25.18	37.38
Snub dodecahedral	452	600	Triangle-Triangle	15.53	15.53	15.82
			Triangle-Pentagon	15.53	23.24	27.07

all the synthesized Fulleroid-like Archimedean deployable mechanisms are of 1-DOF mechanisms.

4. Mobility and Kinematics of the Fulleroid-like Archimedean DPMs

Considering the properties of the eight-bar linkage addressed in Section 2 and the constructed Fulleroid-like Archimedean DPMs in Section 3, mobility and kinematics of the Archimedean DPMs are investigated in this section. Referring to the Kirchhoff's circulation law [38], the instantaneous relative motion of the links can be identified from the linear combination of screw sets. Hence, mobility of the two presented deployable mechanisms can be investigated and verified as long as the screw-loop equations of the mechanisms are established. In this section, based on the Fulleroid-like deployable mechanisms, constraint graphs are sketched and constraint matrices of the mechanisms are formulated; leading to the ranks of the null-space of the mechanisms. The nullity of the constraint matrix gives mobility of the mechanisms in every configuration. In addition, kinematic analysis and simulation of the two synthesized deployable mechanisms are carried out and presented.

4.1. Constraints Matrix and Mobility Analysis of the Fulleroid-like Deployable Cuboctahedral Mechanism

Figure 10 shows the Fulleroid-like deployable cuboctahedral mechanism in an arbitrary configuration with a reference coordinate system attached at the virtual centre of the mechanism. The origin is at point O, with the x-axis passing through the centroid of square facet component V_9, the y-axis passing through the square facet component V_{14}, and the z-axis passing through the square facet component V_{12}.

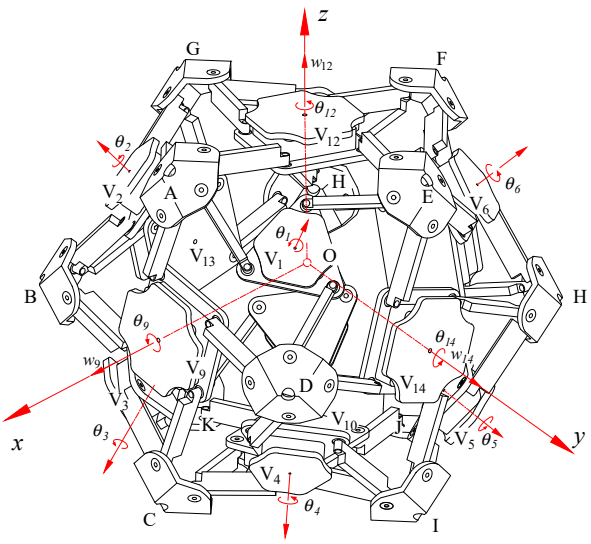

Figure 10: Geometry of a Fulleroid-like deployable cuboctahedral mechanism.

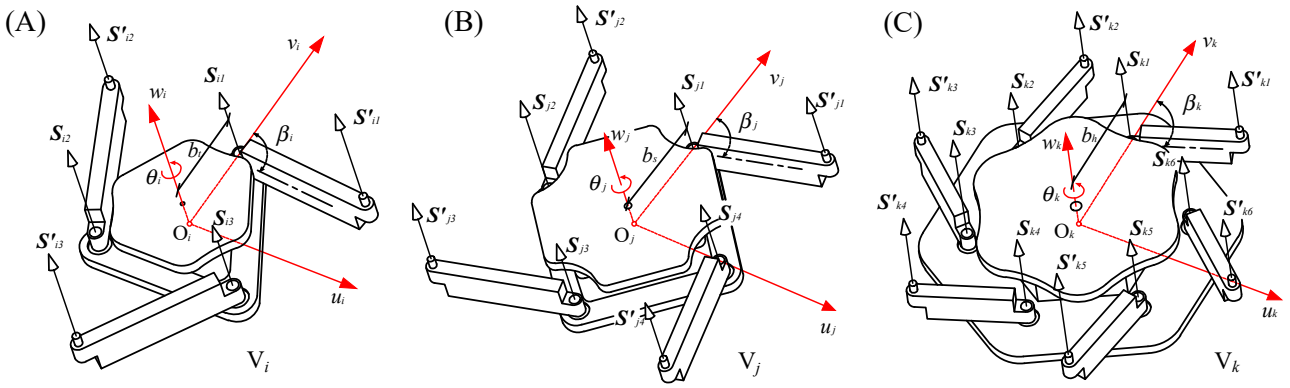

Figure 11: (A)(B)(C) respectively represents joint screws in three different facet component.

In each triangular facet component V_i $(i = 1, 2, 3, \cdots, 8)$, a local coordinate frame $\{u_i, v_i, w_i\}$ is established with its origin O_i locating at the center of the ith equilateral triangular facet component as shown in Fig. 11(A), where the w_i-axis is collinear with OO_i (referring to Fig. 10), the u_i-axis is parallel to one side of the triangular facet. b_t is the distance between O_i and the axis of joint. d_t means the distance between O and O_i. On the square facet components V_j $(j = 9, 10, 11, \cdots, 14)$, the local coordinate frame $\{u_j, v_j, w_j\}$ is established with origin O_j locating at the center of the jth square facet component as shown in Fig. 11(B). In this local coordinate system, the w_j-axis is aligned with OO_j (referring to Fig. 10), the u_k-axis is normal to one side of the square facet component and therefore the v_k-axis is perpendicular to the adjacent edge. The distance between O_k and the axis of joint is b_s, and the distance between O and O_j is d_s.

Since the lengths of all links in Fulleroid-like deployable mechanism are of the same, denoted as l, every edge of the triangular facet component and the square facet component of the Fulleroid-like deployable cuboctahedral mechanism is l. According to the geometric relations in Fig. 11(A) and (B), there exist $b_t = l/\sqrt{3}$, $\beta_i = \arcsin\left(b_t \sin\theta_i / l\right)$ for the triangular facet component, and $b_s = l/\sqrt{2}$, $\beta_j = \arcsin\left(b_s \sin\theta_j / l\right)$ for the square facet component.

Based on Fig. 11(A), joint screws on every individual equilateral triangular component can be derived by referring to their associated local coordinate systems as

$$
\begin{cases}
\boldsymbol{S}_{i1} = \left[\begin{array}{cccccc} 0 & 0 & 1 & b_t & 0 & 0 \end{array}\right]^{\mathrm{T}} \\
\boldsymbol{S}'_{i1} = \left[\begin{array}{cccccc} 0 & 0 & 1 & b_t + l\cos\beta_i & -l\sin\beta_i & 0 \end{array}\right]^{\mathrm{T}} \\
\boldsymbol{S}_{i2} = \left[\begin{array}{cccccc} 0 & 0 & 1 & -\dfrac{b_t}{2} & \dfrac{\sqrt{3}b_t}{2} & 0 \end{array}\right]^{\mathrm{T}} \\
\boldsymbol{S}'_{i2} = \left[\begin{array}{cccccc} 0 & 0 & 1 & -\dfrac{b_t + \left(\cos\beta_i - \sqrt{3}\sin\beta_i\right) l}{2} & \dfrac{\sqrt{3}b_t + l\left(\sqrt{3}\cos\beta_i + \sin\beta_i\right)}{2} & 0 \end{array}\right]^{\mathrm{T}} \\
\boldsymbol{S}_{i3} = \left[\begin{array}{cccccc} 0 & 0 & 1 & -\dfrac{b_t}{2} & -\dfrac{\sqrt{3}b_t}{2} & 0 \end{array}\right]^{\mathrm{T}} \\
\boldsymbol{S}'_{i3} = \left[\begin{array}{cccccc} 0 & 0 & 1 & -\dfrac{b_t + l\left(\cos\beta_i + \sqrt{3}\sin\beta_i\right)}{2} & \dfrac{\sqrt{3}b_t + l\left(\sqrt{3}\cos\beta_i - \sin\beta_i\right)}{2} & 0 \end{array}\right]^{\mathrm{T}}
\end{cases} \tag{23}
$$

And joint screws on every individual square facet component (see Fig. 11(B)) can be calculated relative to the corresponding local coordinate systems as

$$
\begin{cases}
\boldsymbol{S}_{j1} = \left[\begin{array}{cccccc} 0 & 0 & 1 & b_s & 0 & 0 \end{array}\right]^{\mathrm{T}} \\
\boldsymbol{S}'_{j1} = \left[\begin{array}{cccccc} 0 & 0 & 1 & b_s + l\cos\beta_j & -l\sin\beta_j & 0 \end{array}\right]^{\mathrm{T}} \\
\boldsymbol{S}_{j2} = \left[\begin{array}{cccccc} 0 & 0 & 1 & 0 & b_s & 0 \end{array}\right]^{\mathrm{T}} \\
\boldsymbol{S}'_{j2} = \left[\begin{array}{cccccc} 0 & 0 & 1 & l\sin\beta_j & b_s + l\cos\beta_j & 0 \end{array}\right]^{\mathrm{T}} \\
\boldsymbol{S}_{j3} = \left[\begin{array}{cccccc} 0 & 0 & 1 & -b_s & 0 & 0 \end{array}\right]^{\mathrm{T}} \\
\boldsymbol{S}'_{j3} = \left[\begin{array}{cccccc} 0 & 0 & 1 & -b_s - l\cos\beta_j & 0 & 0 \end{array}\right]^{\mathrm{T}} \\
\boldsymbol{S}_{j4} = \left[\begin{array}{cccccc} 0 & 0 & 1 & 0 & -b_s & 0 \end{array}\right]^{\mathrm{T}} \\
\boldsymbol{S}'_{j4} = \left[\begin{array}{cccccc} 0 & 0 & 1 & -l\sin\beta_j & -b_s - l\cos\beta_j & 0 \end{array}\right]^{\mathrm{T}}
\end{cases} \tag{24}
$$

The first subscript $i = 1, 2, 3, \cdots, 8$ in Eqn. (23) indicate the number of triangular facet component. In Eqn. (24), the first subscript $j = 6, 7, 8, \cdots, 14$ means the number of square facet component.

Equation (23) gives the joint screws of the joints embedded in the local coordinate systems in the triangular facet components, these joint screws can be transformed to the reference coordinate system by an adjoint transformation matrix $(\mathbf{A}d_T)_t = \left[\begin{array}{cc} \mathbf{R}_i & \mathbf{0} \\ \tilde{\boldsymbol{p}}_i\mathbf{R}_i & \mathbf{R}_i \end{array}\right]$ with $\mathbf{R}_i$ being the rotation matrix and $\tilde{\boldsymbol{p}}_i$ being a skew-symmetric matrix representation of vector $\boldsymbol{p}_i$ which presents the displacement of point O_i with respect to point O in the reference coordinate system. Similarly, the joint screws for the joints in the local coordinate systems of the square facet components, i.e. Eqn. (24), can be transformed to the reference coordinate system

through matrix $(\mathbf{A}d_T)_s = \begin{bmatrix} \mathbf{R}_j & \mathbf{0} \\ \tilde{\boldsymbol{p}}_j\mathbf{R}_j & \mathbf{R}_j \end{bmatrix}$ with $\mathbf{R}_j$ and $\boldsymbol{p}_j$, Where $\mathbf{R}_j$ is a rotation matrix and $\boldsymbol{p}_j$ is a vector from point O to point O_j. Referring to Fig. 11(A) and (B), $\mathbf{R}_i$, $\mathbf{R}_j$ and $\boldsymbol{p}_i$, $\boldsymbol{p}_j$ are able to obtained and listed in Appendix A.

Further, by referring to Euler's formula in use of mechanical networks [39], the mechanism owns twenty-four independent loops which can be counted by sketching the constraint graph, as listed in Appendix B(A). Further, based on this graph, the constraint matrix of the deployable cuboctahedral mechanism is organized as

$$\mathbf{M}_c = \begin{bmatrix} \mathbf{M}_{c1} & \mathbf{M}_{c2} \end{bmatrix} \tag{25}$$

with

$$\mathbf{M}_{c1} = \begin{bmatrix} \mathbf{0}_{12\times6} & \mathbf{M}_{12} & \mathbf{M}_{13} & \mathbf{0}_{12\times6} & \mathbf{0}_{12\times6} & \mathbf{0}_{12\times6} & \mathbf{M}_{17} \\ \mathbf{M}_{21} & \mathbf{0}_{12\times6} & \mathbf{0}_{12\times6} & \mathbf{M}_{24} & \mathbf{M}_{25} & \mathbf{M}_{26} & \mathbf{0}_{12\times6} \end{bmatrix} \tag{26}$$

$$\mathbf{M}_{c2} = \begin{bmatrix} \mathbf{M}_{18} & \mathbf{M}_{19} & \mathbf{M}_{1-10} & \mathbf{M}_{1-11} & \mathbf{M}_{1-12} & \mathbf{M}_{1-13} & \mathbf{0}_{12\times8} \\ \mathbf{0}_{12\times6} & \mathbf{M}_{29} & \mathbf{M}_{2-10} & \mathbf{M}_{2-11} & \mathbf{M}_{2-12} & \mathbf{0}_{12\times8} & \mathbf{M}_{2-14} \end{bmatrix} \tag{27}$$

where elements $\mathbf{M}_{12}$, $\mathbf{M}_{13}$, $\mathbf{M}_{17}$, $\mathbf{M}_{18}$, $\mathbf{M}_{19}$, $\mathbf{M}_{21}$, $\mathbf{M}_{24}$, $\mathbf{M}_{25}$ and $\mathbf{M}_{26}$ are 12×6 matrices, while $\mathbf{M}_{1-10}$, $\mathbf{M}_{1-11}$, $\mathbf{M}_{1-12}$, $\mathbf{M}_{1-13}$, $\mathbf{M}_{29}$, $\mathbf{M}_{2-10}$, $\mathbf{M}_{2-11}$, $\mathbf{M}_{2-12}$ and $\mathbf{M}_{2-14}$ are 12×8 matrices. Hence, this constraint matrix $\mathbf{M}_c$ is a 144×96 one and detailed matrices can be found in Appendix C. Mobility of the mechanism is determined and identified by the dimension of nullity of the constraint matrix $\mathbf{M}_c$ as

$$m = \dim\left(N(\mathbf{M}_c)\right) = 1 \tag{28}$$

Further, by modelling in Solidworks® as shown in Fig. 6, by given one angular input, the motion simulation indicated that the mechanism has one degree of mobility. Above analysis proves that mobility of the Fulleroid-like deployable cuboctahedral mechanism is one, which means it is an overconstrained mechanism. This method can also been used to calculate the mobility of the truncated tetrahedral mechanism as follows.

4.2. Constraints Matrix and Mobility Analysis of the Fulleroid-like Deployable Truncated Tetrahedral Mechanism

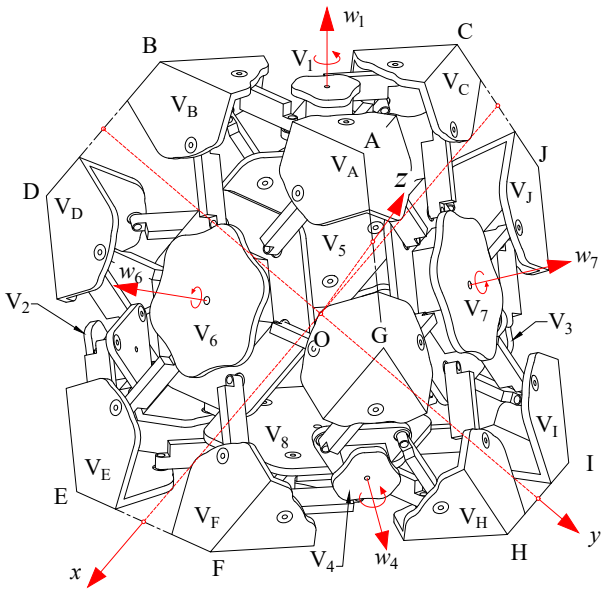

Figure 12: Geometry of Fulleroid-like deployable truncated tetrahedral mechanism.

An arbitrary configuration of the proposed Fulleroid-like deployable truncated tetrahedral mechanism is shown in Fig. 12. For the convenience purpose, a global coordinate system is attached to the mechanism as a reference system with its origin O being located at the virtual centre, and the x-axis, y-axis and z-axis respectively passing through three pairs of middle points (x-axis for edges EF and CJ, y-axis for edges BD and IH, and z-axis for edges AG and KL). Similar to the previous analysis, place a local coordinate system $\{u_i, v_i, w_i\}$ on the ith triangular facet component ($i = 1, 2, 3, 4$) as illustrated in Fig. 11(A). Figure 11(C) illustrates the joint screws on an individual hexagonal facet component, a local coordinate system $\{u_k, v_k, w_k\}$ is attached with its origin O_k locating at the centre of kth hexagonal component ($k = 5, 6, 7, 8$). The v_k-axis passes through one of the vertices of the hexagonal component. The lengths of all the links, in the hexagonal facet component and in the triangular facet component, are all l, the distance between O_k and the axis of the joint is b_h, the distance between O and O_k is d_h.

Joint screws on each hexagonal component (see Fig. 11(C)) can be calculated as

$$
\begin{cases}
\boldsymbol{S}_{k1} = \begin{bmatrix} 0 & 0 & 1 & l & 0 & 0 \end{bmatrix}^{\mathrm{T}} \\
\boldsymbol{S}'_{k1} = \begin{bmatrix} 0 & 0 & 1 & l + l\cos\beta_k & -l\sin\beta_k & 0 \end{bmatrix}^{\mathrm{T}} \\
\boldsymbol{S}_{k2} = \begin{bmatrix} 0 & 0 & 1 & \frac{1}{2}l & \frac{\sqrt{3}}{2}l & 0 \end{bmatrix}^{\mathrm{T}} \\
\boldsymbol{S}'_{k2} = \begin{bmatrix} 0 & 0 & 1 & \frac{1}{2}l + l\sin\left(\beta_k + \frac{\pi}{6}\right) & \frac{\sqrt{3}}{2}l + l\cos\left(\beta_k + \frac{\pi}{6}\right) & 0 \end{bmatrix}^{\mathrm{T}} \\
\boldsymbol{S}_{k3} = \begin{bmatrix} 0 & 0 & 1 & -\frac{1}{2}l & \frac{\sqrt{3}}{2}l & 0 \end{bmatrix}^{\mathrm{T}} \\
\boldsymbol{S}'_{k3} = \begin{bmatrix} 0 & 0 & 1 & -\frac{1}{2}l - l\cos\left(\beta_k + \frac{\pi}{3}\right) & \frac{\sqrt{3}}{2}l + l\sin\left(\beta_k + \frac{\pi}{3}\right) & 0 \end{bmatrix}^{\mathrm{T}} \\
\boldsymbol{S}_{k4} = \begin{bmatrix} 0 & 0 & 1 & -l & 0 & 0 \end{bmatrix}^{\mathrm{T}} \\
\boldsymbol{S}'_{k4} = \begin{bmatrix} 0 & 0 & 1 & -l - l\cos\beta_k & l\sin\beta_k & 0 \end{bmatrix}^{\mathrm{T}} \\
\boldsymbol{S}_{k5} = \begin{bmatrix} 0 & 0 & 1 & -\frac{1}{2}l & -\frac{\sqrt{3}}{2}l & 0 \end{bmatrix}^{\mathrm{T}} \\
\boldsymbol{S}'_{k5} = \begin{bmatrix} 0 & 0 & 1 & -\frac{1}{2}l - l\sin\left(\beta_k + \frac{\pi}{6}\right) & -\frac{\sqrt{3}}{2}l - l\cos\left(\beta_k + \frac{\pi}{6}\right) & 0 \end{bmatrix}^{\mathrm{T}} \\
\boldsymbol{S}_{k6} = \begin{bmatrix} 0 & 0 & 1 & \frac{1}{2}l & -\frac{\sqrt{3}}{2}l & 0 \end{bmatrix}^{\mathrm{T}} \\
\boldsymbol{S}'_{k6} = \begin{bmatrix} 0 & 0 & 1 & \frac{1}{2}l + l\cos\left(\beta_k + \frac{\pi}{3}\right) & -\frac{\sqrt{3}}{2}l - l\sin\left(\beta_k + \frac{\pi}{3}\right) & 0 \end{bmatrix}^{\mathrm{T}}
\end{cases}
\tag{29}
$$

where the subscript k indicting the number of hexagonal facet component. From the geometry information in Fig. 11(C), there exists $b_h = l$ and $\beta_k = \theta_k$.

In the Fulleroid-like deployable truncated tetrahedral mechanism, the adjoint transformation

matrices for transforming the joint screws from the local coordinate frames in the triangular facet component and the hexagonal facet component to the reference coordinate system are given as $(\mathbf{A}d_T)_t = \begin{bmatrix} \mathbf{R}_i & \mathbf{0} \\ \tilde{\boldsymbol{p}}_i\mathbf{R}_i & \mathbf{R}_i \end{bmatrix}$ and $(\mathbf{A}d_T)_h = \begin{bmatrix} \mathbf{R}_k & \mathbf{0} \\ \tilde{\boldsymbol{p}}_k\mathbf{R}_k & \mathbf{R}_k \end{bmatrix}$, respectively. Where $\mathbf{R}_i$, $\mathbf{R}_k$, $\boldsymbol{p}_i$, and $\boldsymbol{p}_k$ are calculated and listed in Appendix D.

Similarly, the constraint graph is sketched as illustrated in Appendix B(B); Hence the constraint matrix can be derived as

$$\mathbf{M}'_c = \begin{bmatrix} \mathbf{M}'_{c1} & \mathbf{M}'_{c2} \end{bmatrix} \tag{30}$$

where

$$\mathbf{M}'_{c1} = \begin{bmatrix} \mathbf{M}_{11} & \mathbf{M}_{12} & \mathbf{0}_{9\times6} & \mathbf{M}_{14} \\ \mathbf{0}_{9\times6} & \mathbf{M}_{22} & \mathbf{M}_{23} & \mathbf{M}_{24} \end{bmatrix} \tag{31}$$

$$\mathbf{M}'_{c2} = \begin{bmatrix} \mathbf{M}_{15} & \mathbf{M}_{16} & \mathbf{M}_{17} & \mathbf{0}_{9\times12} \\ \mathbf{M}_{25} & \mathbf{M}_{26} & \mathbf{M}_{27} & \mathbf{M}_{28} \end{bmatrix} \tag{32}$$

in Eqns. (31) and (32), the elements $\mathbf{M}_{11}$, $\mathbf{M}_{12}$, $\mathbf{M}_{14}$, $\mathbf{M}_{22}$, $\mathbf{M}_{23}$ and $\mathbf{M}_{24}$ are 9×6 matrices. $\mathbf{M}_{15}$, $\mathbf{M}_{16}$, $\mathbf{M}_{17}$, $\mathbf{M}_{25}$, $\mathbf{M}_{26}$, $\mathbf{M}_{27}$ and $\mathbf{M}_{28}$ are 9×12 matrices. More details of the constraint matrices are listed in Appendix E. Hence, $\mathbf{M}'_c$ is a 108×72 matrix. Then through programming in symbolic system such as Matlab®, it gives mobility of the mechanism as $m = \dim(\mathrm{Null}(\mathbf{M}'_c)) = 1$.

Further, by modelling in Solidworks®, one can run the simulation for testing the mobility of the stereo mechanism by giving only one angular variation input on any link around its corresponding revolute joint, it turns out that the mechanism performs the prospective motion such that the triangular and hexagonal facet components are able to operate screw motion and the vertex components can carry out strict reciprocating straight-line motion. Therefore, the mobility of the mechanism is one.

The above analysis clearly reveals that both the deployable cuboctahedral and truncated tetrahedral mechanisms has only one mobility. Hence, these two mechanisms are both over-constrained mechanisms. Without loss of generality, this method can be generalized to the mobility analysis of other Fulleroid-like Archimedean DPMs in the group. All the mechanisms synthesized in this paper have a single degree of freedom.

4.3. Kinematics and Motion Simulations of the Fulleroid-like Archimedean DPMs

In this section, kinematics of the Sarrus-like overcontrained eight-bar linkage is investigated first. Further to the structure equation of the linkage derived in Section 2, by implanting the eight-bar linkage into the Archimedean polyhedral base, e.g. the truncated tetrahedral base illustrated in Fig. 13, we aim to investigate the kinematic performance of the eight-bar linkage within the polyhedral base. As shown in Fig. 13, the eight-bar linkage is integrated into the base along the edge GF which is shared by a hexagonal face and a triangular face. The linkage is in an arbitrary configuration which means the links A_1B_1, A_2B_2, B_1C_1, B_2C_2, C_1D_1 and C_2D_2 are not in the same positions as initially indicated in Fig. 8(A).

Then we transform the coordinate system $\{x_0, y_0, z_0\}$ to the fix coordinate system $\{x, y, z\}$ of the polyhedral base with the origin O being the centroid of the truncated tetrahedral base. By pre-multiplying this transformation with the structure equations derived in Section 2.4, it is found that if the joint angles meet the requirements of $\alpha_{11} = \alpha_{24}$, $\alpha_{12} = \alpha_{23}$ and $\alpha_{13} = \alpha_{22}$, motion of the eight-bar linkage can be characterized. Given the structure parameters and implementing the equations in Section 2.4 in computer program, the motion of the eight-bar linkage is simulated and illustrated in Fig. 14. From Fig. 14, it can be seen that traces of joints B_1 and C_1 are double helix line in 3-dimensional space as well as the joints B_2 and C_2 do (seeing the grass green lines). The simulation is well verified in the truncated tetrahedral

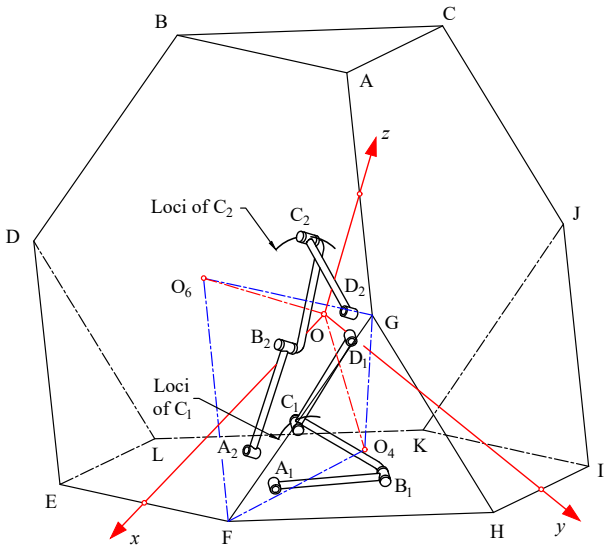

Figure 13: Only one proposed eight-bar linkage in the regular truncated tetrahedron base.

mechanism model in Fig. 15, which shows four typical configurations, including the fully-folded configuration (Fig. 15(A)) and fully-expanded configuration (Fig. 15(D)). In Fig. 15, four blue sliders indicate the motion traces intersected at point O, which is the centre of the red truncated tetrahedron base. Regarding the fully-folded configuration, joints A_1, C_1 are overlapped, so do the joints B_2, D_2. These simulations evidently reveal that the two triangular components (one side of each the triangular component formed by link 3 and link 7) are able to achieve screw motions around associated virtual axes and the vertex components (formed by V_1 and V_2 contain joints A_1, A_2 and D_1, D_2) implement radially reciprocating motions along their associated virtual axes.

This single-loop motion simulation hence verifies that the proposed eight-bar linkage is able to operate the motions as expected for synthesizing Fulleroid-like mechanisms. This motion analysis can then be generalized to the motion analysis of the whole group of Fulleroid-like Archimedean DPMs.

For the Fulleroid-like deployable cuboctahedral mechanism, Fig. 16 displays the position relationship between a triangular facet component and a square facet component. In the figure, the w_i-axis and the w_j-axis are respectively the virtual axes of the triangular facet component and the adjacent square facet component. Point O is the virtual centre of the mechanism, O_i is the centre point of the equilateral triangular facet component, O_j is the centre point of the square facet component, and O′ is the vertex point in the vertex component which is located at the intersection of the joint axes. The angle between OO′ and OO_i is γ_1 which is constant, with the value 54.74°; and the angle between OO′ and OO_j is γ_2, with a constant value 45°. According to the property of the proposed deployable cuboctahedral mechanism, it is expected that, when the vertex component performs reciprocating straight line along OO′, the triangular and square facet components carry out screw motion around axes w_i and w_j respectively with rotation angles θ_i and θ_j, and displacements d_t and d_s. Hence, when the length of the link l is given, referring to Fig. 11(A), it has

$$O'O_i = b_t \cos\theta_i + l\cos\beta_i \tag{33}$$

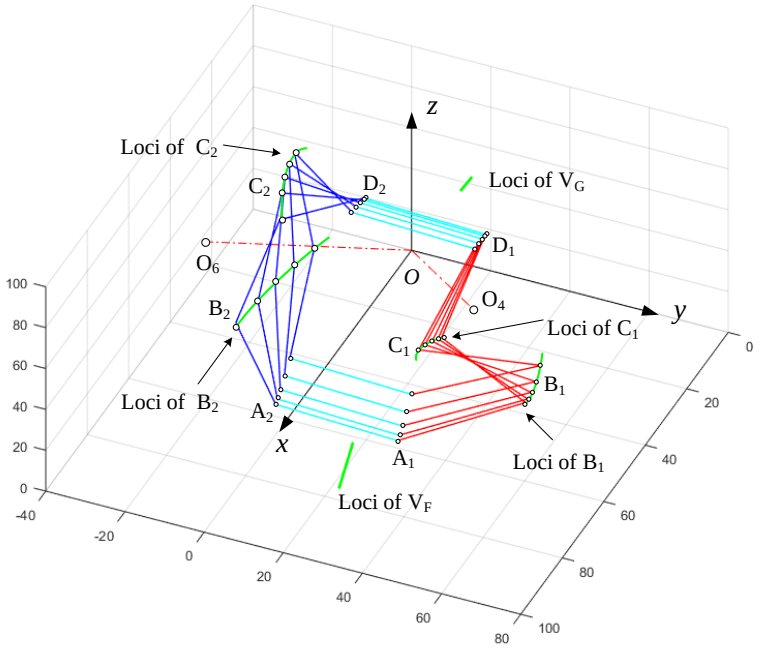

Figure 14: Single-loop motion simulation of truncated tetrahedral mechanism.

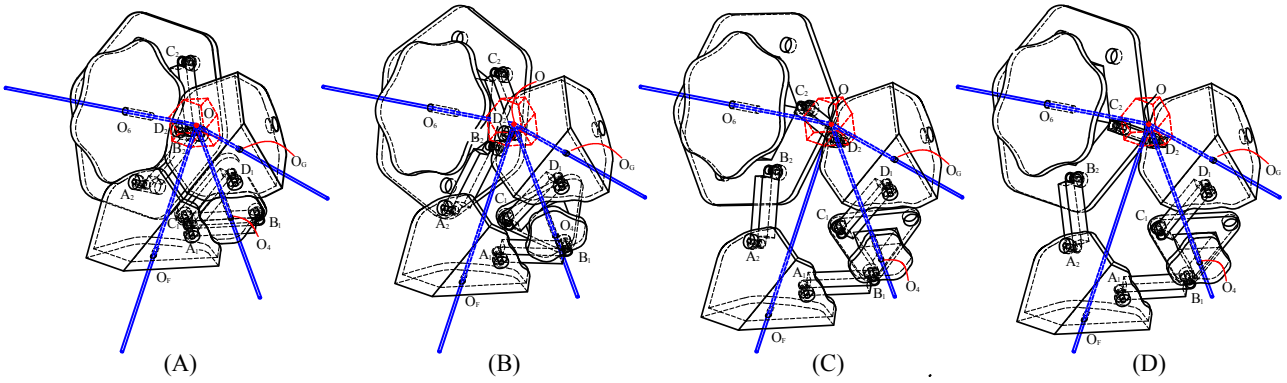

Figure 15: Single-loop motion demonstration of truncated tetrahedral mechanism.

Since $\beta_i = \arcsin(b_t \sin\theta_i / l)$, and $b_t = \dfrac{\sqrt{3}l}{3}$, Eq. (33) can be further derived as

$$\mathrm{O'O}_i = \frac{\sqrt{3}}{3} l \left(\cos\theta_i + \sqrt{2 + \cos^2\theta_i}\right) \tag{34}$$

Hence, referring to Fig. 11, in the right-angled triangle $\mathrm{OO}_i\mathrm{O'}$, $\mathrm{OO'}$ can be obtained as

$$\mathrm{OO'} = \frac{\mathrm{O'O}_i}{\sin\gamma_1} = \frac{\sqrt{3}l\left(\cos\theta_i + \sqrt{2 + \cos^2\theta_i}\right)}{3\sin\gamma_1} \tag{35}$$

Similarly, in the right-angled triangle $\mathrm{OO'O}_j$, there exists

$$\mathrm{O'O_j} = b_s \cos\theta_j + l\cos\beta_j = \frac{\sqrt{2}l\left(\cos\theta_j + \sqrt{1 + \cos^2\theta_j}\right)}{2} \tag{36}$$

where $\beta_j = \arcsin(b_s \sin\theta_i / l)$, and $b_s = \dfrac{\sqrt{2}l}{2}$, and such that $\mathrm{OO'}$ can also be expressed as

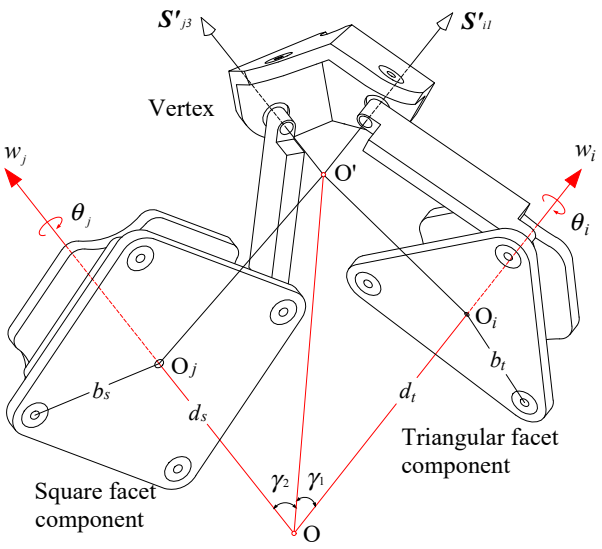

Figure 16: Geometry of square facet component and triangular facet component.

$$\mathrm{OO}' = \frac{\mathrm{O}'\mathrm{O_j}}{\sin\gamma_2} = \frac{\sqrt{2}l\left(\cos\theta_j + \sqrt{1+\cos^2\theta_j}\right)}{2\sin\gamma_2} \tag{37}$$

According to the property of the cuboctahedral base, it has $\sin\gamma_1 = \sqrt{6}/3$ and $\sin\gamma_2 = \sqrt{2}/2$, hence from Eqns. (35) and (37), it yields

$$\cos\theta_i + \sqrt{2+\cos^2\theta_i} = \sqrt{2}\left(\cos\theta_j + \sqrt{1+\cos^2\theta_j}\right) \tag{38}$$

In addition, the displacements d_t and d_s can be expressed with respect to the rotation angles as

$$d_t = \frac{\mathrm{O}'\mathrm{O}_i}{\tan\gamma_1} = \frac{\sqrt{3}l\left(\cos\theta_i + \sqrt{2+\cos^2\theta_i}\right)}{3\tan\gamma_1} = \frac{\sqrt{6}l\kappa_1}{6} \tag{39}$$

and

$$d_s = \frac{\mathrm{O}'\mathrm{O}_j}{\tan\gamma_2} = \frac{\sqrt{2}l\left(\cos\theta_i + \sqrt{1+\cos^2\theta_i}\right)}{2\tan\gamma_1} = \frac{\sqrt{2}l\kappa_2}{2} \tag{40}$$

where, $\kappa_1 = \cos\theta_i + \sqrt{2+\cos^2\theta_i}$ and $\kappa_2 = \cos\theta_j + \sqrt{1+\cos^2\theta_j}$.

Using the angle relationship in Eqn. (38) and the displacements in Eqns. (39) and (40) together and kinematics for the eight-bar linkage, kinematic analysis of the cuboctahedral deployable mechanism can be derived and simulated as shown in Fig. 17. The figure indicates that the triangular and square components are able to achieve screw motion around their associated virtual axes and the vertex components can operate reciprocating straight line motion along their corresponding virtual axes. With the feature of well-implemented radially reciprocating movement, the relationship between the velocities (triangular facet component and square facet component) and two angles θ_i and θ_j of the actuated components is discussed as follow.

According to the geometry of the cuboctahedral mechanism, Position vectors of all the triangular facet components can be denoted as from $\mathbf{P}_1$ to $\mathbf{P}_8$, and position vectors of all the square facet components can be named as $\mathbf{P}_9$ throughout $\mathbf{P}_{14}$. Keep the global reference coordinate system unchanged, seeing in Fig.18, position vector of points P_1 can be obtained from Appendix A as

$$\mathbf{P}_1 = \boldsymbol{A}_1 d_t \tag{41}$$

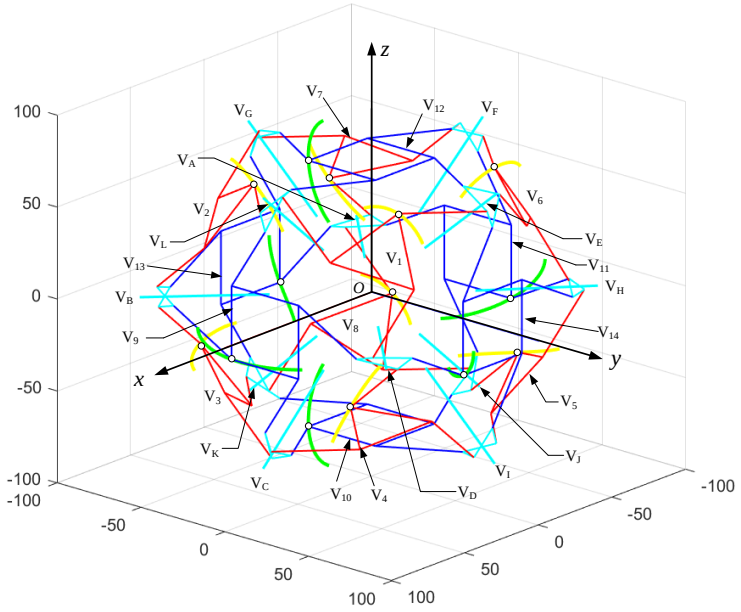

Figure 17: Motion simulation (working trajectory) of the Fulleroid-like deployable cuboctahedral mechanism.

where $\boldsymbol{A}_1 = \left[\begin{array}{ccc} \frac{\sqrt{3}}{3} & \frac{\sqrt{3}}{3} & \frac{\sqrt{3}}{3} \end{array}\right]^{\mathrm{T}}$.

Then, position vector of point P_2 can be obtained as $\mathbf{P}_2 = \boldsymbol{A}_2 d_t$ with $\boldsymbol{A}_2 = \left[\begin{array}{ccc} \frac{\sqrt{3}}{3} & \frac{-\sqrt{3}}{3} & \frac{\sqrt{3}}{3} \end{array}\right]^{\mathrm{T}}$. Similarly, $\mathbf{P}_3 = \boldsymbol{A}_3 d_t$ with $\boldsymbol{A}_3 = \left[\begin{array}{ccc} \frac{\sqrt{3}}{3} & \frac{-\sqrt{3}}{3} & \frac{-\sqrt{3}}{3} \end{array}\right]^{\mathrm{T}}$, $\mathbf{P}_4 = \boldsymbol{A}_4 d_t$ with $\boldsymbol{A}_4 = \left[\begin{array}{ccc} \frac{\sqrt{3}}{3} & \frac{\sqrt{3}}{3} & \frac{-\sqrt{3}}{3} \end{array}\right]^{\mathrm{T}}$, $\mathbf{P}_5 = \boldsymbol{A}_5 d_t$ with $\boldsymbol{A}_5 = \left[\begin{array}{ccc} \frac{-\sqrt{3}}{3} & \frac{\sqrt{3}}{3} & \frac{-\sqrt{3}}{3} \end{array}\right]^{\mathrm{T}}$, $\mathbf{P}_6 = \boldsymbol{A}_6 d_t$ with $\boldsymbol{A}_6 = \left[\begin{array}{ccc} \frac{-\sqrt{3}}{3} & \frac{\sqrt{3}}{3} & \frac{\sqrt{3}}{3} \end{array}\right]^{\mathrm{T}}$, $\mathbf{P}_7 = \boldsymbol{A}_7 d_t$ with $\boldsymbol{A}_7 = \left[\begin{array}{ccc} \frac{-\sqrt{3}}{3} & \frac{-\sqrt{3}}{3} & \frac{\sqrt{3}}{3} \end{array}\right]^{\mathrm{T}}$ and $\mathbf{P}_8 = \boldsymbol{A}_8 d_t$ with $\boldsymbol{A}_8 = \left[\begin{array}{ccc} \frac{-\sqrt{3}}{3} & \frac{-\sqrt{3}}{3} & \frac{-\sqrt{3}}{3} \end{array}\right]^{\mathrm{T}}$.

Regarding the square facet components, position vector of point P_9 can be obtained as

$$\mathbf{P}_9 = \boldsymbol{A}_9 d_s \tag{42}$$

where $\boldsymbol{A}_9 = \left[\begin{array}{ccc} 1 & 1 & 0 \end{array}\right]^{\mathrm{T}}$.

Similarly, the position vectors for the rest points on the square facet components can be derived as $\mathbf{P}_{10} = \boldsymbol{A}_{10} d_s$ with $\boldsymbol{A}_{10} = \left[\begin{array}{ccc} 0 & 0 & -1 \end{array}\right]^{\mathrm{T}}$, $\mathbf{P}_{11} = \boldsymbol{A}_{11} d_s$ with $\boldsymbol{A}_{11} = \left[\begin{array}{ccc} -1 & 0 & 0 \end{array}\right]^{\mathrm{T}}$, $\mathbf{P}_{12} = \boldsymbol{A}_{12} d_s$ with $\boldsymbol{A}_{12} = \left[\begin{array}{ccc} 0 & 0 & 1 \end{array}\right]^{\mathrm{T}}$, $\mathbf{P}_{13} = \boldsymbol{A}_{13} d_s$ with $\boldsymbol{A}_{13} = \left[\begin{array}{ccc} 0 & -1 & 0 \end{array}\right]^{\mathrm{T}}$, $\mathbf{P}_{14} = \boldsymbol{A}_{14} d_s$ with $\boldsymbol{A}_{14} = \left[\begin{array}{ccc} 0 & 1 & 0 \end{array}\right]^{\mathrm{T}}$.

It is found from above analysis that the deployable Fulleroid-like cuboctahedral mechanism has one degree of freedom, if the actuated component starts rotating, the displacements of all the centres of the 12 facet components can be determined. The forward kinematic analysis of the mechanism consists of determination of the velocities of the centroids of the facet components for a given velocity of the active triangular facet component $\dot{\theta}_i$. Take differential of the position vectors $\mathbf{P}_1$ to $\mathbf{P}_8$, the velocities of points P_1 to P_8 can be obtained and Jacobian can be given as

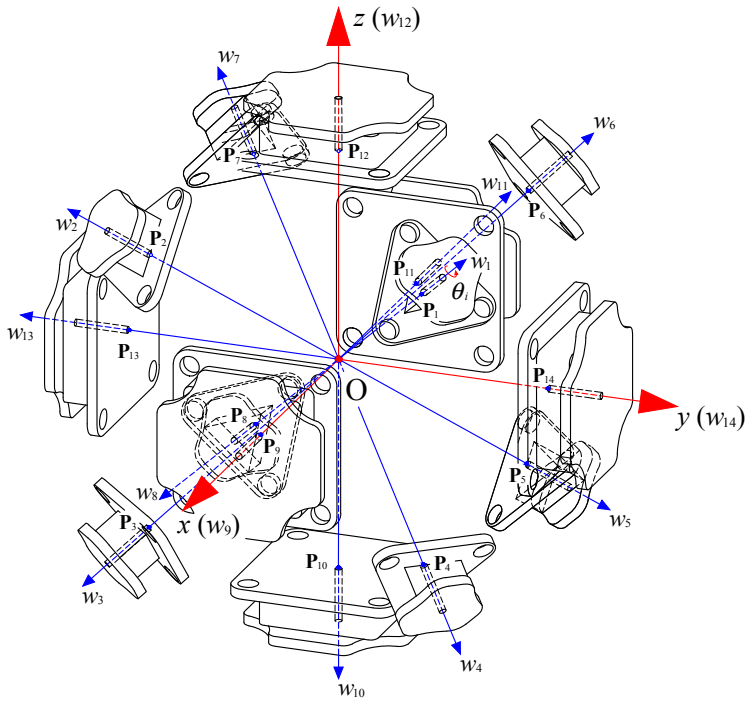

Figure 18: Position analysis of all the facet components of the Fulleroid-like deployable cuboctahedral mechanism.

$$\begin{bmatrix} \boldsymbol{v}_{p1} \\ \boldsymbol{v}_{p2} \\ \boldsymbol{v}_{p3} \\ \boldsymbol{v}_{p4} \\ \boldsymbol{v}_{p5} \\ \boldsymbol{v}_{p6} \\ \boldsymbol{v}_{p7} \\ \boldsymbol{v}_{p8} \end{bmatrix} = \begin{bmatrix} \boldsymbol{J}_1 & & & & & & & \\ & \boldsymbol{J}_2 & & & & & & \\ & & \boldsymbol{J}_3 & & & & & \\ & & & \boldsymbol{J}_4 & & & & \\ & & & & \boldsymbol{J}_5 & & & \\ & & & & & \boldsymbol{J}_6 & & \\ & & & & & & \boldsymbol{J}_7 & \\ & & & & & & & \boldsymbol{J}_8 \end{bmatrix} \dot{\theta}_i \tag{43}$$

where sub-matrixes $\boldsymbol{J}_1$, $\boldsymbol{J}_2$, $\boldsymbol{J}_3$, $\boldsymbol{J}_4$, $\boldsymbol{J}_5$, $\boldsymbol{J}_6$, $\boldsymbol{J}_7$, $\boldsymbol{J}_8$ of the Jacobian matrix can be obtained by taking time differential of the corresponding position vectors. For the suqare facet components, by following the same method, the velocities of points P_9 to P_{14} can be obtained and Jacobian can be given as

$$\begin{bmatrix} \boldsymbol{v}_{p9} \\ \boldsymbol{v}_{p10} \\ \boldsymbol{v}_{p11} \\ \boldsymbol{v}_{p12} \\ \boldsymbol{v}_{p13} \\ \boldsymbol{v}_{p14} \end{bmatrix} = \begin{bmatrix} \boldsymbol{J}_9 & & & & & \\ & \boldsymbol{J}_{10} & & & & \\ & & \boldsymbol{J}_{11} & & & \\ & & & \boldsymbol{J}_{12} & & \\ & & & & \boldsymbol{J}_{13} & \\ & & & & & \boldsymbol{J}_{14} \end{bmatrix} \dot{\theta}_j \tag{44}$$

where sub-matrixes $\boldsymbol{J}_9$, $\boldsymbol{J}_{10}$, $\boldsymbol{J}_{11}$, $\boldsymbol{J}_{12}$, $\boldsymbol{J}_{13}$, $\boldsymbol{J}_{14}$ of the Jacobian matrix can be obtained by taking time differential of the corresponding position vectors $\mathbf{P}_9$ to $\mathbf{P}_{14}$.

It can be found that the resultant velocities of triangular facet components are the same, and the resultant velocities of square facet components are the same, and the relationship of $\dot{\theta}_i$ and $\dot{\theta}_j$ can be obtained from Eqn. (38). Further, once any position of the centroid point of the facet components of the mechanism is given, the input rotation angle θ_i or θ_j can be obtained. From any position vectors, θ_i and θ_j can be expressed as the functions of the positions of the centroid points. For example, when the position of point P_1 is known the rotation angle θ_i can

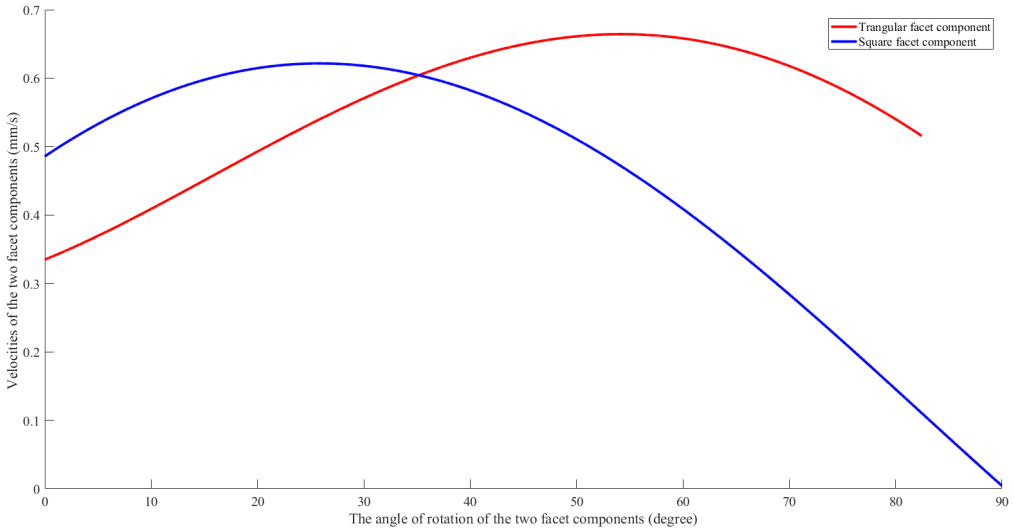

Figure 19: Velocities of two different components along the associated virtual axes of the Fulleroid-like deployable cuboctahedral mechanism.

be represented as

$$\theta_i = \arccos\left(\frac{\left(p_{1x} - \frac{\sqrt{2}}{6}l\right)^2 - 2}{2\left(p_{1x} - \frac{\sqrt{2}}{6}l\right)}\right) \tag{45}$$

where p_{1x} is the x-component of vector $\mathbf{P}_1$ and l is the link length as aforementioned.

According to the geometry of the cuboctahedral mechanism, we can have $d_t(n)$, $d_s(n)$, where n means the angle of actuated component. Particularly, the ranges of rotation angle of triangular actuated component and square actuated component are $[0°, 82.46°]$ and $[0°, 90°]$, respectively. The angular velocity is $1°/s$. The displacement increments of d_t and d_s along their virtual axes in the n-th second is

$$\delta d_t(n) = d_t(n) - d_t(n-1) \tag{46}$$

and

$$\delta d_s(n) = d_s(n) - d_s(n-1) \tag{47}$$

Thus for each second, the velocities of the two different components can be written as $v_t(n)$ and $v_s(n)$. With the parameter of link length is 40 mm, the velocities of two components along their own moving axes in a specified actuated angle from fully folded state to fully expanded state is programmed and presented in Fig. 19.

Similarly, Fig. 20 represents the relationship of a triangular facet component and a hexagonal facet component in the deployable truncated tetrahedral mechanism. The w_i-axis and w_k-axis are respectively the virtual axes of the two components intersecting at the virtual centre O. O′ is the intersect point of the screw axes in the vertex component, O_i is the centre point of the triangular component and O_k is the centre point of the hexagonal component. Angle γ_1 is a constant with value 29.5° and angle γ_2 equals 58.52°. Similar to the above derivations for the cuboctahedral mechanism, referring to Figs. 11 (A) and (C) there exist $O'O_i = b_t \cos\theta_i + l\cos\beta_i$ and $O'O_k = b_h \cos\theta_k + l\cos\beta_k$, such that the OO′ can be obtained in the right-angled triangle OO_iO' the same as the one in Eqn. (35), and in the right-angled triangle OO_kO' as

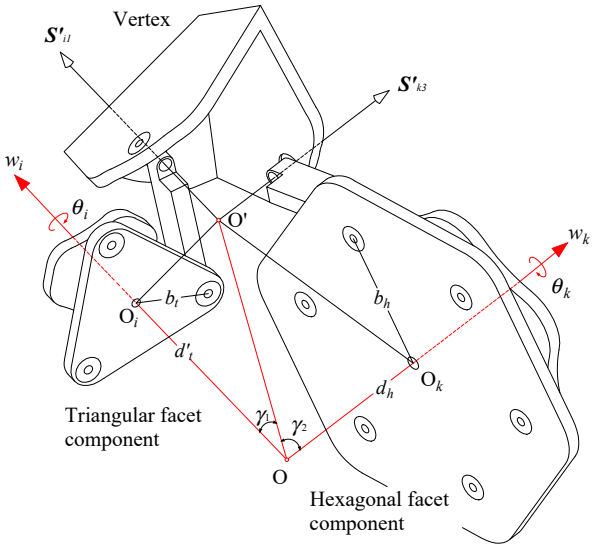

Figure 20: Geometry of triangular facet component and hexagonal facet component.

$$\mathrm{OO}' = \frac{\mathrm{O}_k\mathrm{O}'}{\sin\gamma_2} = \frac{2l\cos\theta_k}{\sin\gamma_2} \tag{48}$$

with the relations that $b_h = l$ and $\beta_k = \theta_k$.

Equating Eqns. (35) and (48), it yields $\dfrac{\sqrt{3}l\left(\cos\theta_i + \sqrt{2+\cos^2\theta_i}\right)}{3\sin\gamma_1} = \dfrac{2l\cos\theta_k}{\sin\gamma_2}$. With $\sin\gamma_1$=0.492 and $\sin\gamma_2 = 0.853$, the relation between angles θ_i and θ_k in the truncated tetrahedral mechanism can be given as

$$\frac{1}{2}\left(\cos\theta_i + \sqrt{2+\cos^2\theta_i}\right) = \cos\theta_k \tag{49}$$

Further, the displacements d'_t and d_h can be formulated as

$$d'_t = \frac{\mathrm{O}'\mathrm{O}_i}{\tan\gamma_1} = \frac{\sqrt{3}l\left(\cos\theta_i + \sqrt{2+\cos^2\theta_i}\right)}{3\tan\gamma_1} = 1.02l\kappa_1 \tag{50}$$

and

$$d_h = \frac{\mathrm{O}'\mathrm{O}_k}{\tan\gamma_2} = \frac{2l\cos\theta_k}{1.633} = 1.225l\kappa_3 \tag{51}$$

where κ_1 is the same one as Eq. (39) and $\kappa_3 = \cos\theta_k$.

By referring to Fig. 21, position vectors denoted as $\mathbf{P}_1$ throughout $\mathbf{P}_8$ represent the positions of all facet components of the deployable Fulleroid-like truncated tetrahedral mechanism. Taking the same approach, position vector of point P_1 can be deduced as

$$\mathbf{P}_1 = \boldsymbol{A}_1 d'_t \tag{52}$$

where $\boldsymbol{A}_1 = \begin{bmatrix} \frac{-\sqrt{3}}{3} & \frac{-\sqrt{3}}{3} & \frac{\sqrt{3}}{3} \end{bmatrix}^{\mathrm{T}}$.

Subsequently, position vector of point P_2 can be obtained as $\mathbf{P}_2 = \boldsymbol{A}_2 d'_t$ with $\boldsymbol{A}_2 = \begin{bmatrix} \frac{\sqrt{3}}{3} & \frac{-\sqrt{3}}{3} & \frac{-\sqrt{3}}{3} \end{bmatrix}^{\mathrm{T}}$. Similarly, $\mathbf{P}_3 = \boldsymbol{A}_3 d'_t$ with $\boldsymbol{A}_3 = \begin{bmatrix} \frac{-\sqrt{3}}{3} & \frac{\sqrt{3}}{3} & \frac{-\sqrt{3}}{3} \end{bmatrix}^{\mathrm{T}}$, $\mathbf{P}_4 = \boldsymbol{A}_4 d_t$ with $\boldsymbol{A}_4 = \begin{bmatrix} \frac{\sqrt{3}}{3} & \frac{\sqrt{3}}{3} & \frac{\sqrt{3}}{3} \end{bmatrix}^{\mathrm{T}}$. Further, for the hexagonal facet components, $\mathbf{P}_5 = \boldsymbol{A}_5 d_h$ with

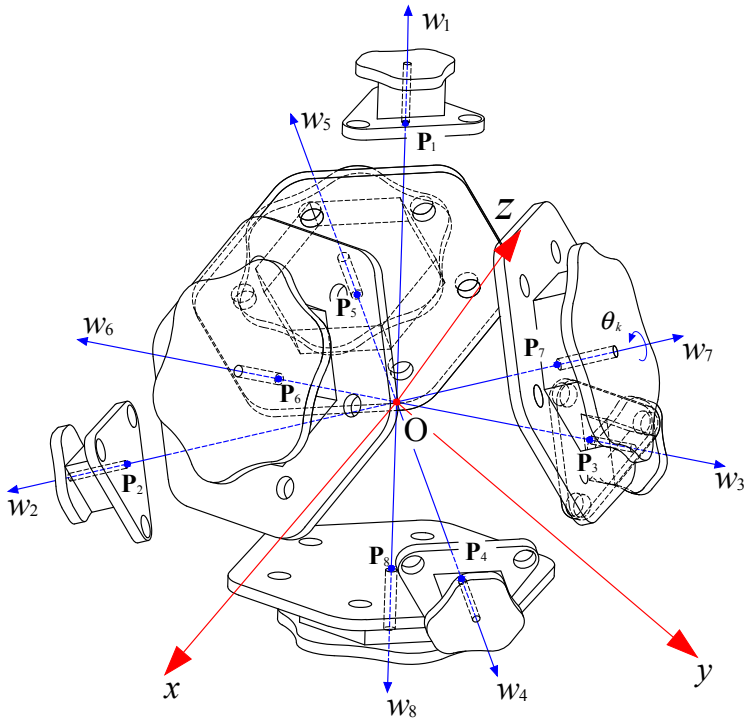

Figure 21: Position analysis of all the facet components of the Fulleroid-like deployable truncated tetrahedral mechanism.

$\boldsymbol{A}_5 = \begin{bmatrix} \frac{-\sqrt{3}}{3} & \frac{-\sqrt{3}}{3} & \frac{-\sqrt{3}}{3} \end{bmatrix}^{\mathrm{T}}$, $\mathbf{P}_6 = \boldsymbol{A}_6 d_h$ with $\boldsymbol{A}_6 = \begin{bmatrix} \frac{\sqrt{3}}{3} & \frac{-\sqrt{3}}{3} & \frac{\sqrt{3}}{3} \end{bmatrix}^{\mathrm{T}}$, $\mathbf{P}_7 = \boldsymbol{A}_7 d_h$ with $\boldsymbol{A}_7 = \begin{bmatrix} \frac{-\sqrt{3}}{3} & \frac{\sqrt{3}}{3} & \frac{\sqrt{3}}{3} \end{bmatrix}^{\mathrm{T}}$ and $\mathbf{P}_8 = \boldsymbol{A}_8 d_h$ with $\boldsymbol{A}_8 = \begin{bmatrix} \frac{\sqrt{3}}{3} & \frac{\sqrt{3}}{3} & \frac{-\sqrt{3}}{3} \end{bmatrix}^{\mathrm{T}}$.

Similarly, taking differential of the position vectors $\mathbf{P}_1$ to $\mathbf{P}_4$, the velocities of points P_1 to P_4 can be obtained and Jacobian can be given as

$$\begin{bmatrix} \boldsymbol{v}_{p1} \\ \boldsymbol{v}_{p2} \\ \boldsymbol{v}_{p3} \\ \boldsymbol{v}_{p4} \end{bmatrix} = \begin{bmatrix} \boldsymbol{J}_1 & & & \\ & \boldsymbol{J}_2 & & \\ & & \boldsymbol{J}_3 & \\ & & & \boldsymbol{J}_4 \end{bmatrix} \dot{\theta}_i \tag{53}$$

where sub-matrixes $\boldsymbol{J}_1$, $\boldsymbol{J}_2$, $\boldsymbol{J}_3$, $\boldsymbol{J}_4$ of the Jacobian matrix can be obtained by taking time differential of the corresponding position vectors. For the hexagonal facet components, by following the same method, the velocities of points P_5 to P_8 can be obtained and Jacobian can be given as

$$\begin{bmatrix} \boldsymbol{v}_{p5} \\ \boldsymbol{v}_{p6} \\ \boldsymbol{v}_{p7} \\ \boldsymbol{v}_{p8} \end{bmatrix} = \begin{bmatrix} \boldsymbol{J}_5 & & & \\ & \boldsymbol{J}_6 & & \\ & & \boldsymbol{J}_7 & \\ & & & \boldsymbol{J}_8 \end{bmatrix} \dot{\theta}_k \tag{54}$$

where sub-matrixes $\boldsymbol{J}_5$, $\boldsymbol{J}_6$, $\boldsymbol{J}_7$, $\boldsymbol{J}_8$ and $\boldsymbol{J}_{13}$ of the Jacobian matrix can be obtained by taking time differential of the corresponding position vectors $\mathbf{P}_5$ to $\mathbf{P}_8$.

By referring the relationship of $\dot{\theta}_i$ and $\dot{\theta}_k$ from Eqn. (49), once any position of the centroid point of the facet components of the truncated tetrahedral mechanism is given, the input rotation angle θ_i or θ_k can be obtained. From any position vectors, θ_i and θ_k can be expressed as the functions of the positions of the centroid points. For example, the most convenient one can be obtained from position of point P_7, when the position vector $\mathbf{P}_7$ is known the rotation

angle θ_k can be represented as

$$\theta_k = \arccos\left(\frac{\sqrt{2}p_{7z}}{l}\right) \tag{55}$$

where p_{7z} is the z-component of vector $\mathbf{P}_7$ with l being denoted as the link length.

With Eqns. (49), (50) and (51) and the kinematics of the eight-bar linkage and given the structure parameters, motion and velocities of the triangular facet component and hexagonal facet component of the Fulleroid-like deployable truncated tetrahedral mechanism can be characterised and simulated as illustrated in Figs. 22 and 23. Figures indicate that in the deployable truncated tetrahedral mechanism, the eight components all operate screw motion around the associated virtual axes with real-time velocities and twelve vertices are able to achieve radially reciprocating motion along their associated virtual axes.

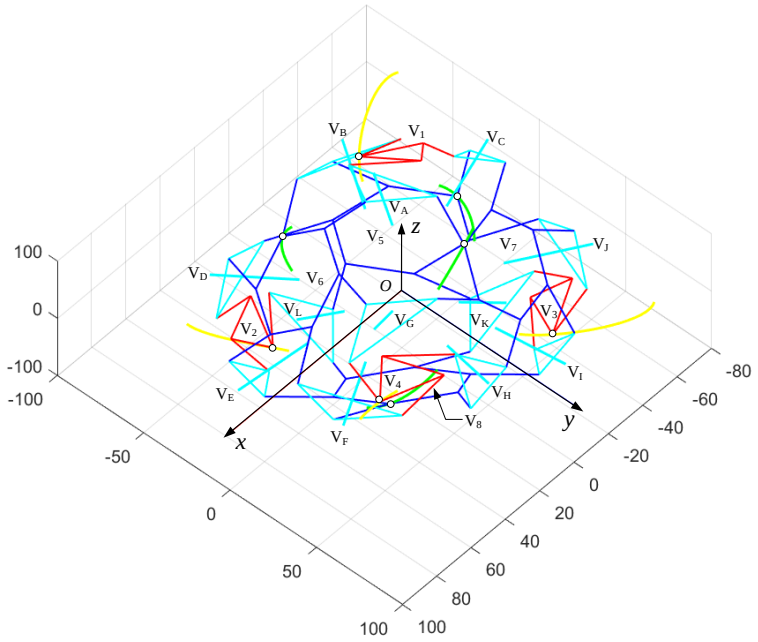

Figure 22: Motion simulation (working trajectory) of the Fulleroid-like deployable truncated tetrahedral mechanism.

Further, referring to the mobility and motion analysis above, it is found that the two deployable Fulleroid-like Archimedean mechanisms are both mobility one and if the rotation angle (θ_i or θ_j in the Fulleroid-like deployable cuboctahedral mechanism and θ_i or θ_k in the Fulleroid-like deployable truncated tetrahedral mechanism) is given, the displacement of all the centres of the facet components of those deployable Fulleroid-like Archimedean mechanisms can be determined. It also has been well verified that the double helix motions of all joints in those mechanisms comply with the geometric constraint presented in Section 2. It is noted that, for the concerning of bifurcation/multifurcation behaviour, which is generally unavoidable for deployable structures [40], the unexpected motions will lead the mechanical structure into any one of the bifurcation paths. the multifurcation of the proposed mechanisms can be solved by the adding constraint gears to couple the rotating of the joints in the same vertex component and facet component as indicated in [24, 28, 40]. However, the mobility of the mechanisms reported in the paper have been investigated using screw theory and their motion paths including the moving traces of each facet components and the representative joints on the facet components are verified by programmed simulations. It is found and proved that by giving only one actuate rotation input, the components will all move as expected, which are translations along their virtual axes. Each single facet component is coplanar with the connected links,

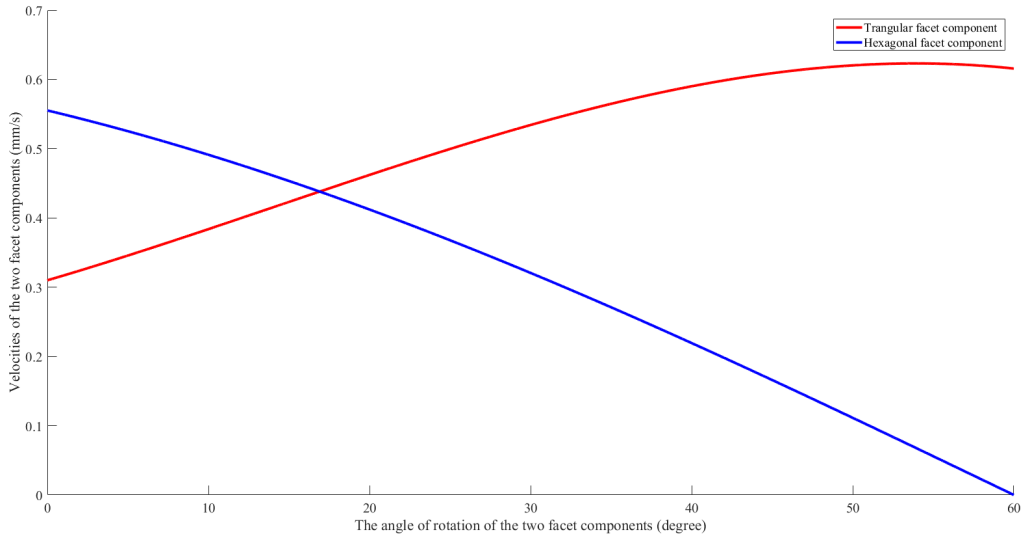

Figure 23: Velocities of two different components along the associated virtual axes of the Fulleroid-like deployable truncated tetrahedral mechanism.

and the links are moving with the facet component toward and backward along the same orientation while the facet components are self-revolving on the axis. The singular positions are very straightforward, are the fully-folded configuration and the fully-expanded configuration, no matter the cuboctahedral mechanism or the truncated tetrahedral mechanism. It is noted that in the fully-expanded configuration of the cuboctahedral mechanism, the distal joint of the link connected to the square facet component has been reached the farthest position while the triangular facet component and its associated links do not reach the farthest position (if reach, the angle between the link and the adjacent edge of triangular facet component should be 120 degree).

By following the same pattern, kinematics of the other eleven deployable Archimedean mechanisms are able to obtained and analysed which helps to reveal the characterizations of Fulleroid-like deployable mechanisms from the constructing point of view. In addition, computation algorithms as presented in [33] can be considered to increase the efficiency of the construction process.

5. Conclusions

An efficient and intuitive approach was presented in this paper for the synthesis and construction of a group of featured Fulleroid-like Archimedean DPMs based on a Sarrus-like overconstrained spatial eight-bar linkage. Structure and mobility of the linkage were briefly introduced and formulated, which clearly verified that the proposed linkage is an overconstrained mechanism like the Sarrus linkage. Then by selecting the cuboctahedron and truncated tetrahedron as example bases, the approach for synthesizing a characteristic features of Fulleroid mechanisms, called Fulleroid-like deployable cuboctahedral mechanism and Fulleroid-like deployable truncated tetrahedral mechanism were presented and illustrated. Further, based on Kirchhoff's circulation law for independent loop using in mechanical networks, mobility of the proposed mechanisms was studied. In order to demonstrate the motion performance of the proposed eight-bar linkage and the Fulleroid-like Archimedean DPMs, kinematics of the linkages was researched and stated with numerical simulations. The results clearly indicate that the eight-bar linkage is able to performs double-helix motion (link 3 and link 7) integrated with straight-line motion (movable platform denoted as link V_2); and for all the synthesized and constructed Fulleroid-like Archimedean DPMs in this paper, all the facet components that involved, are able to operate screw motion around their associated virtual axes, and all the

vertex components are capable of performing radially reciprocating motion along their corresponding virtual axes. The proposed deployable mechanisms have great potential applications in reconfigurable robotics, deployable architectures and expendable space exploring devices.

6. References

[1] E. Rivas-Adrover, Deployable Structures, Laurence King Publishing, London, 2015.

[2] W. Cao, D. Yang, H. Ding, A new family of deployable mechanisms derived from two-layer and two-loop spatial linkages with five revolute pair coupling chains, Journal of Mechanisms and Robotics 9 (6) (2017) 061016.

[3] M. Goldberg, New five-bar and six-bar linkages in three dimensions, Transactions of the ASME 65 (1943) 649–661.

[4] R. B. Fuller, Synergetics,explorations in the geometry of thinking, Macmillan Publishing Co.Inc., New York, NY, 1979.

[5] H. F. Verheyen, Expandable polyhedral structures based on dipolygonids, in: Proc. 3rd Int. conf. Space Structures, Elsevier, London, UK, 1984.

[6] H. F. Verheyen, The complete set of jitterbug transformers and the analysis of their motion, Computers & Mathematics with Applications 17 (1-3) (1989) 203–250.

[7] H. Stachel, The heureka-polyhedron, in: Intuitive Geometry, Vol. 63, Colloq. Math. Soc. Jnos Bolyai, North-Holland, Amsterdam., 1994, pp. 447–459.

[8] K. Wohlhart, Heureka octahedron and brussels folding cube as special cases of the turning tower, in: Proc. the Sixth IFToMM International Symposium on Linkages and Computer Aided Design Methods, Bucharest, Romania, 1993.

[9] K. Wohlhart, New overconstrained spheroidal linkages, in: Proc. the Ninth World Congress on the Theory of Machines and Mechanisms, Milano, Italy, 1995.

[10] O. Röschel, Overconstrained mechanisms based on trapezohedra, in: Proceedings of the 15th International Conference on Geometry and Graphics (ICGG 2012), 2012, pp. 629–637.

[11] O. Röschel, A fulleroid-like mechanism based on the cube, Journal for Geometry and Graphics 16 (1) (2012) 19–27.

[12] K. Wohlhart, Deformable cages, in: 10th World Congress on the Theory of Machines and Mechanisms, Oulo, Finland, 1999, pp. 683–688.

[13] K. Wohlhart, Regular polyhedral linkages, in: Proc. 3rd IFToMM International Workshop on Computational Kinematics, Seoul, South Korea, 2001, p. 22, http://www-sop.inria.fr/coprin/EJCK/Vol1-1/.

[14] K. Wohlhart, Irregular polyhedral linkages, in: Proc. the Eleventh World Congress in Mechanism and Machine Science, 2004.

[15] C. Hoberman, Geared expanding structures (2008).

[16] C. M. Gosselin, D. Gagnon-Lachance, Expandable polyhedral mechanisms based on polygonal one-degree-of-freedom faces, Proc. IMechE Part C: J. Mechanical Engineering Science 220 (2006) 1011–1018.

[17] T. Laliberté, C. M. Gosselin, Polyhedra with articulated faces, in: Proc. of the 12th IFToMM World Congress, 2007.

[18] G. C.M, G.-L. D, Expandable polyhedral mechanisms based on polygonal one-degree-of-freedom faces, in: Proceedings of the Institution of Mechanical Engineers, Part C: Journal of Mechanical Engineering Science, 2006, pp. 1011–1018.

[19] S. K. Agrawal, S. Kumar, M. Yim, Polyhedral single degree-of freedom expanding structures: design and prototypes, Transactions of the ASME: Journal of Mechanical Design 124 (9) (2002) 473–478.

[20] J. Wang, X. Kong, Deployable mechanisms constructed by connecting orthogonal bricard linkages, 8r or 10r single-loop linkages using s joints, Mechanism and Machine Theory 120 (2018) 178–191.

[21] R. Li, Y. an Yao, X. Kong, Reconfigurable deployable polyhedral mechanism based on extended parallelogram mechanism, Mechanism and Machine Theory 116 (2017) 467–480.

[22] F. Kovács, T. Tarnai, P. W. Fowler, G. S. D., A class of expandable polyhedral structures, International Journal of Solids and Structures 41 (2004) 1119–1137.

[23] G. Wei, J. S. Dai, A spatial eight-bar linkage and its association with the deployable platonic mechanisms, Journal of Mechanisms and Robotics 6 (2) (2014) 021010–021010–9.

[24] G. Wei, X. Ding, J. S. Dai, Mobility and geometric analysis of the hoberman switch-pitch ball and its variant, Transactions of the ASME: Journal of Mechanisms and Robotics 2 (3) (2010) 031010.

[25] G. Wei, J. S. Dai, Synthesis of a family of regular deployable polyhedral mechanisms, in: J. Lenarčič, M. Husty (Eds.), Latest Advances in Robot Kinematics, Springer, 2012, pp. 123–130.

[26] G. Wei, J. S. Dai, Overconstrained mechanisms with radially reciprocating motion, in: J. Lenarčič, M. Stanišić (Eds.), Advances in Robot Kinematics: Motion in Man and Machine, Springer, 2010.

[27] G. Wei, J. S. Dai, Synthesis and construction of a family of one-dof highly overconstrained deployable polyhedral mechanisms (dpms), in: 2012 Conference proceeding of Design Engineering Technical Conferences & Computers and Information in Engineering Conference, 2012.

[28] G. Wei, Y. Chen, J. S. Dai, Synthesis, mobility and multifurcation of deployable polyhedral mechanisms with radially reciprocating motion, Transactions of the ASME: Journal of Mechanical Design 136 (11).

[29] Y. Chen, S. D. Guest, P. Fowler, J. Feng, Two-orbit switch-pitch structures, Journal of the International Association for Shell and Spatial Structures 53 (2012) 157–162.

[30] Y. Chen, J. Feng, Y. Liu, A group-theoretic approach to the mobility and kinematic of symmetric over-constrained structures, Mechanism and Machine Theory 105 (2016) 91 – 107.

[31] S. D. Guest, P. W. Fowler, A symmetry-extended mobility rule, Mechanism and Machine Theory 40 (9) (2005) 1002–1014.

[32] Y. Chen, J. Feng, Improved symmetry method for the mobility of regular structures using graph products, Journal of Structural Engineering 142 (9) (2016) 04016051.

[33] Y. Chen, P. Sareh, J. Feng, Q. Sun, A computational method for automated detection of engineering structures with cyclic symmetries, Computers and Structures 191 (2017) 153–164.

[34] K. Wohlhart, Kinematics and dynamics of the fulleroid, Multibody Systems Dynamies 1 (1997) 241–258.

[35] H. Xiu, K. Wang, G. Wei, L. Ren, J. S. Dai, A sarrus-like overconstrained eight-bar linkage and its associated fulleroid-like platonic deployable mechanisms, Proc. IMechE Part C: J Mechanical Engineering Science (2018) 1–22DOI: 10.1177/0954406218816343.

[36] P. F. Sarrus, Note sur la transformation des mouvements rectilignes alternatifs, en mouvements circulaires; et reciproquement, Academie des Sciences 36 (1853) 1036–1038.

[37] K. H. Hunt, Kinematic Geometry of Mechanisms, Oxford University Press, Clarendon, Oxford, UK, 1978.

[38] T. Davies, Kirchhoff's circulation law applied to multi-loop kinematic chains, Mechanism and Machine Theory 16 (3) (1981) 171–183.

[39] L.-W. Tsai, Mechanism Design: Enumeration of Kinematic Structures According to Function, CRC Press, Corporate Blvd., Boca Raton, Florida, 2001.

[40] Y. Chen, J. Feng, S. Zhi, Lower-order symmetric mechanism modes and bifurcation behavior of deployable bar structures with cyclic symmetry, International Journal of Solids and Structures 139-140 (2018) 1 – 14.

Appendix A.

$$\mathbf{R}_1 = \begin{bmatrix} 0.107\sin\theta_i - 0.809\cos\theta_i & -0.107\cos\theta_i - 0.809\sin\theta_i & 0.577 \\ 0.498\cos\theta_i + 0.647\sin\theta_i & 0.498\sin\theta_i - 0.647\cos\theta_i & 0.577 \\ 0.312\cos\theta_i - 0.755\sin\theta_i & 0.755\cos\theta_i + 0.312\sin\theta_i & 0.577 \end{bmatrix} \tag{A.1}$$

$$\mathbf{R}_2 = \begin{bmatrix} 0.647\sin\theta_i + 0.498\cos\theta_i & 0.647\cos\theta_i + 0.498\sin\theta_i & 0.577 \\ 0.809\cos\theta_i - 0.107\sin\theta_i & 0.107\cos\theta_i + 0.809\sin\theta_i & -0.577 \\ 0.312\cos\theta_i - 0.755\sin\theta_i & 0.755\cos\theta_i + 0.312\sin\theta_i & 0.577 \end{bmatrix} \tag{A.2}$$

$$\mathbf{R}_3 = \begin{bmatrix} 0.498\cos\theta_i + 0.647\sin\theta_i & 0.498\sin\theta_i - 0.647\cos\theta_i & 0.577 \\ 0.755\sin\theta_i - 0.312\cos\theta_i & -0.755\cos\theta_i - 0.312\sin\theta_i & -0.577 \\ 0.809\cos\theta_i - 0.107\sin\theta_i & 0.107\cos\theta_i + 0.809\sin\theta_i & -0.577 \end{bmatrix} \tag{A.3}$$

$$\mathbf{R}_4 = \begin{bmatrix} 0.312\cos\theta_i - 0.755\sin\theta_i & 0.755\sin\theta_i + 0.312\cos\theta_i & 0.577 \\ 0.498\cos\theta_i + 0.647\sin\theta_i & 0.498\cos\theta_i - 0.647\sin\theta_i & 0.577 \\ 0.809\cos\theta_i - 0.107\sin\theta_i & 0.107\cos\theta_i + 0.809\sin\theta_i & -0.577 \end{bmatrix} \tag{A.4}$$

$$\mathbf{R}_5 = \begin{bmatrix} 0.107\sin\theta_i - 0.809\cos\theta_i & 0.107\cos\theta_i + 0.809\sin\theta_i & -0.577 \\ 0.755\sin\theta_i - 0.312\cos\theta_i & 0.755\cos\theta_i + 0.312\sin\theta_i & -0.577 \\ 0.647\sin\theta_i + 0.498\cos\theta_i & 0.647\cos\theta_i - 0.498\sin\theta_i & 0.577 \end{bmatrix} \tag{A.5}$$

$$\mathbf{R}_6 = \begin{bmatrix} -0.498\cos\theta_i - 0.647\sin\theta_i & 0.647\cos\theta_i - 0.498\sin\theta_i & -0.577 \\ -0.809\cos\theta_i - 0.107\sin\theta_i & 0.107\cos\theta_i - 0.809\sin\theta_i & 0.577 \\ 0.312\cos\theta_i - 0.755\sin\theta_i & 0.755\cos\theta_i + 0.312\sin\theta_i & 0.577 \end{bmatrix} \tag{A.6}$$

$$\mathbf{R}_7 = \begin{bmatrix} 0.312\cos\theta_i - 0.755\sin\theta_i & -0.755\cos\theta_i - 0.312\sin\theta_i & -0.577 \\ 0.498\cos\theta_i + 0.647\sin\theta_i & 0.647\cos\theta_i - 0.498\sin\theta_i & -0.577 \\ 0.809\cos\theta_i - 0.107\sin\theta_i & -0.107\cos\theta_i - 0.809\sin\theta_i & 0.577 \end{bmatrix} \tag{A.7}$$

$$\mathbf{R}_8 = \begin{bmatrix} 0.755\sin\theta_i - 0.312\cos\theta_i & -0.755\cos\theta_i - 0.312\sin\theta_i & -0.577 \\ -0.498\cos\theta_i - 0.647\sin\theta_i & 0.647\cos\theta_i - 0.498\sin\theta_i & -0.577 \\ 0.809\cos\theta_i - 0.107\sin\theta_i & 0.107\cos\theta_i + 0.809\sin\theta_i & -0.577 \end{bmatrix} \tag{A.8}$$

$$\mathbf{R}_9 = \begin{bmatrix} 0 & 0 & 1 \\ -\sin\theta_j & -\cos\theta_j & 0 \\ \cos\theta_j & -\sin\theta_j & 0 \end{bmatrix} \tag{A.9}$$

$$\mathbf{R}_{10} = \begin{bmatrix} \sin\theta_j & \cos\theta_j & 0 \\ \cos\theta_j & -\sin\theta_j & 0 \\ 0 & 0 & -1 \end{bmatrix} \tag{A.10}$$

$$\mathbf{R}_{11} = \begin{bmatrix} 0 & 0 & -1 \\ \sin\theta_j & \cos\theta_j & 0 \\ \cos\theta_j & -\sin\theta_j & 0 \end{bmatrix} \tag{A.11}$$

$$\mathbf{R}_{12} = \begin{bmatrix} -\cos\theta_j & \sin\theta_j & 0 \\ -\sin\theta_j & -\cos\theta_j & 0 \\ 0 & 0 & 1 \end{bmatrix} \tag{A.12}$$

$$\mathbf{R}_{13} = \begin{bmatrix} \sin\theta_j & -\cos\theta_j & 0 \\ 0 & 0 & -1 \\ \cos\theta_j & \sin\theta_j & 0 \end{bmatrix} \tag{A.13}$$

$$\mathbf{R}_{14} = \begin{bmatrix} -\sin\theta_j & \cos\theta_j & 0 \\ 0 & 0 & 1 \\ \cos\theta_j & \sin\theta_j & 0 \end{bmatrix} \tag{A.14}$$

$$\boldsymbol{p}_1 = d_t \begin{bmatrix} 0.577 & 0.577 & 0.577 \end{bmatrix}^{\mathrm{T}} \tag{A.15}$$

$$\boldsymbol{p}_2 = d_t \begin{bmatrix} 0.577 & -0.577 & 0.577 \end{bmatrix}^{\mathrm{T}} \tag{A.16}$$

$$\boldsymbol{p}_3 = d_t \begin{bmatrix} 0.577 & -0.577 & -0.577 \end{bmatrix}^{\mathrm{T}} \tag{A.17}$$

$$\boldsymbol{p}_4 = d_t \begin{bmatrix} 0.577 & 0.577 & -0.577 \end{bmatrix}^{\mathrm{T}} \tag{A.18}$$

$$\boldsymbol{p}_5 = d_t \begin{bmatrix} -0.577 & 0.577 & -0.577 \end{bmatrix}^{\mathrm{T}} \tag{A.19}$$

$$\boldsymbol{p}_6 = d_t \begin{bmatrix} -0.577 & 0.577 & 0.577 \end{bmatrix}^{\mathrm{T}} \tag{A.20}$$

$$\boldsymbol{p}_7 = d_t \begin{bmatrix} -0.577 & -0.577 & 0.577 \end{bmatrix}^{\mathrm{T}} \tag{A.21}$$

$$\boldsymbol{p}_8 = d_t \begin{bmatrix} -0.577 & -0.577 & -0.577 \end{bmatrix}^{\mathrm{T}} \tag{A.22}$$

$$\boldsymbol{p}_9 = d_s \begin{bmatrix} 1 & 1 & 0 \end{bmatrix}^{\mathrm{T}} \tag{A.23}$$

$$\boldsymbol{p}_{10} = d_s \begin{bmatrix} 0 & 0 & -1 \end{bmatrix}^{\mathrm{T}} \tag{A.24}$$

$$\boldsymbol{p}_{11} = d_s \begin{bmatrix} -1 & 0 & 0 \end{bmatrix}^{\mathrm{T}} \tag{A.25}$$

$$\boldsymbol{p}_{12} = d_s \begin{bmatrix} 0 & 0 & 1 \end{bmatrix}^{\mathrm{T}} \tag{A.26}$$

$$\boldsymbol{p}_{13} = d_s \begin{bmatrix} 0 & -1 & 0 \end{bmatrix}^{\mathrm{T}} \tag{A.27}$$

$$\boldsymbol{p}_{14} = d_s \begin{bmatrix} 0 & 1 & 0 \end{bmatrix}^{\mathrm{T}} \tag{A.28}$$

Appendix B.

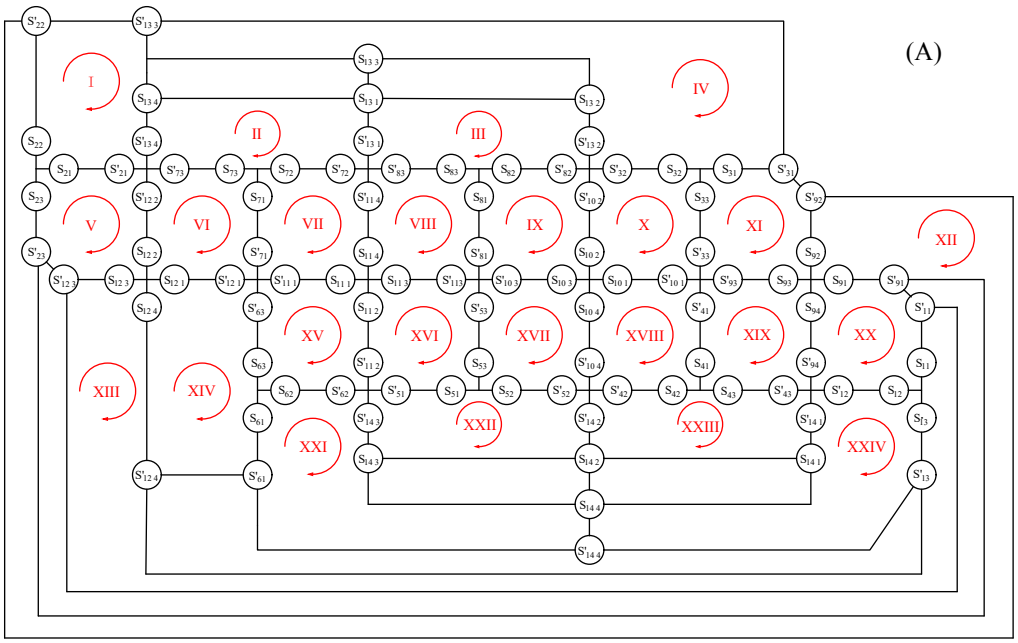

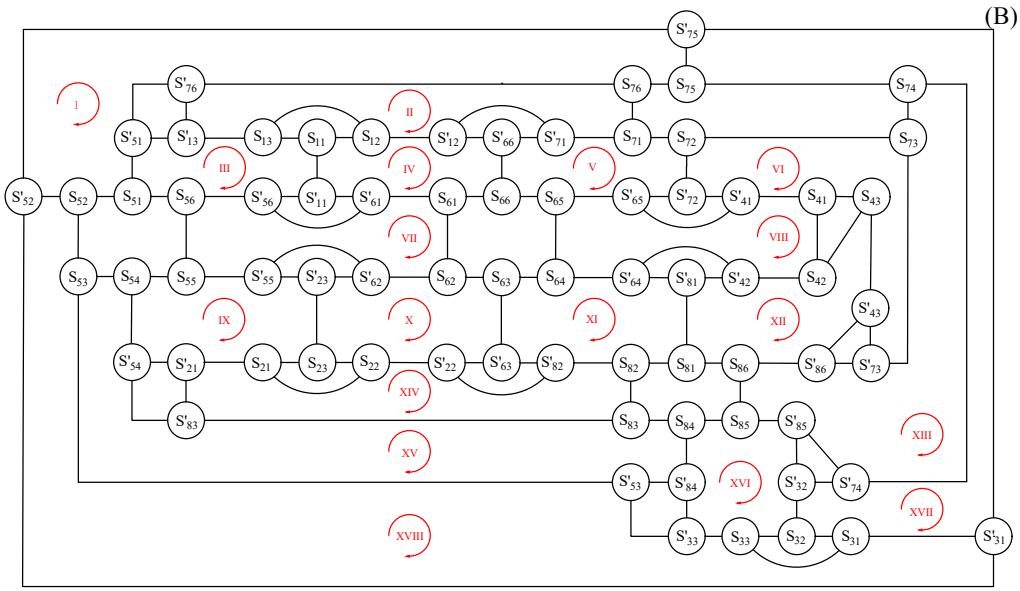
(B)
S'75
S'76
S76
S75
S74
I
II
S'51
S'13
S13
S11
S12
S'12
S'66
S'71
S71
S72
S73
III
IV
V
VI
S'52
S52
S51
S56
S'56
S'11
S'61
S61
S66
S65
S'65
S'72
S'41
S41
S43
VII
VIII
S53
S54
S55
S'55
S'23
S'62
S62
S63
S64
S'64
S'81
S'42
S42
S'43
IX
X
XI
XII
S'54
S'21
S21
S23
S22
S'22
S'63
S'82
S82
S81
S86
S'86
S'73
XIV
S'83
S83
S84
S85
S'85
XIII
XV
S'53
S'84
XVI
S'32
S'74
XVII
XVIII
S'33
S33
S32
S31
S'31

Appendix C.

$$\mathbf{M_{12}}=\begin{bmatrix} \boldsymbol{S}_{21} & \boldsymbol{S}'_{21} & \boldsymbol{S}_{22} & \boldsymbol{S}'_{22} & \mathbf{0} & \mathbf{0} \\ & & \mathbf{0}_{3\times6} & & & \\ -\boldsymbol{S}_{21} & -\boldsymbol{S}'_{21} & \mathbf{0} & \mathbf{0} & \boldsymbol{S}_{23} & \boldsymbol{S}'_{23} \\ & & \mathbf{0}_{6\times6} & & & \\ \mathbf{0} & \mathbf{0} & -\boldsymbol{S}_{22} & -\boldsymbol{S}'_{22} & -\boldsymbol{S}_{23} & -\boldsymbol{S}'_{23} \end{bmatrix} \tag{C.1}$$

$$\mathbf{M}_{13}=\begin{bmatrix} & & \mathbf{0}_{3\times6} & & & \\ \boldsymbol{S}_{31} & \boldsymbol{S}'_{31} & \boldsymbol{S}_{32} & \boldsymbol{S}'_{32} & \mathbf{0} & \mathbf{0} \\ & & \mathbf{0}_{5\times6} & & & \\ \mathbf{0} & \mathbf{0} & -\boldsymbol{S}_{32} & -\boldsymbol{S}'_{32} & \boldsymbol{S}_{33} & \boldsymbol{S}'_{33} \\ -\boldsymbol{S}'_{31} & -\boldsymbol{S}'_{31} & \mathbf{0} & \mathbf{0} & -\boldsymbol{S}_{33} & -\boldsymbol{S}'_{33} \\ \mathbf{0} & \mathbf{0} & \mathbf{0} & \mathbf{0} & \mathbf{0} & \mathbf{0} \end{bmatrix} \tag{C.2}$$

$$\mathbf{M}_{17}=\begin{bmatrix} & \mathbf{0} & \mathbf{0} & \mathbf{0} & \mathbf{0} & \mathbf{0} & \mathbf{0} \\ & \mathbf{0} & \mathbf{0} & \boldsymbol{S}_{72} & \boldsymbol{S}'_{72} & \boldsymbol{S}_{73} & \boldsymbol{S}'_{73} \\ & & & \mathbf{0}_{3\times6} & & & \\ \boldsymbol{S}_{71} & \boldsymbol{S}'_{71} & \mathbf{0} & \mathbf{0} & -\boldsymbol{S}_{73} & -\boldsymbol{S}'_{73} \\ -\boldsymbol{S}_{71} & -\boldsymbol{S}'_{71} & -\boldsymbol{S}_{72} & -\boldsymbol{S}'_{72} & \mathbf{0} & \mathbf{0} \\ & & & \mathbf{0}_{5\times6} & & & \end{bmatrix} \tag{C.3}$$

$$\mathbf{M}_{21}=\begin{bmatrix} \boldsymbol{S}_{11} & \boldsymbol{S}'_{11} & \mathbf{0} & \mathbf{0} & \boldsymbol{S}S_{13} & \boldsymbol{S}'_{13} \\ & & \mathbf{0}_{6\times6} & & & \\ -\boldsymbol{S}_{11} & -\boldsymbol{S}'_{11} & \boldsymbol{S}_{12} & \boldsymbol{S}'_{12} & \mathbf{0} & \mathbf{0} \\ & & \mathbf{0}_{3\times6} & & & \\ \mathbf{0} & \mathbf{0} & -\boldsymbol{S}_{12} & -\boldsymbol{S}'_{12} & -\boldsymbol{S}_{13} & -\boldsymbol{S}'_{13} \end{bmatrix} \tag{C.4}$$

$$\mathbf{M}_{24}=\begin{bmatrix} & & \mathbf{0}_{5\times6} & & & \\ \boldsymbol{S}_{41} & \boldsymbol{S}'_{41} & \boldsymbol{S}_{42} & \boldsymbol{S}'_{42} & \mathbf{0} & \mathbf{0} \\ -\boldsymbol{S}_{41} & -\boldsymbol{S}'_{41} & \mathbf{0} & \mathbf{0} & \boldsymbol{S}_{43} & \boldsymbol{S}'_{43} \\ & & \mathbf{0}_{3\times6} & & & \\ \mathbf{0} & \mathbf{0} & -\boldsymbol{S}_{42} & -\boldsymbol{S}'_{42} & -\boldsymbol{S}_{43} & -\boldsymbol{S}'_{43} \\ \mathbf{0} & \mathbf{0} & \mathbf{0} & \mathbf{0} & \mathbf{0} & \mathbf{0} \end{bmatrix} \tag{C.5}$$

$$\mathbf{M}_{25}=\begin{bmatrix} & & \mathbf{0}_{3\times6} & & & \\ \boldsymbol{S}_{51} & \boldsymbol{S}'_{51} & \mathbf{0} & \mathbf{0} & \boldsymbol{S}_{53} & \boldsymbol{S}'_{53} \\ \mathbf{0} & \mathbf{0} & \boldsymbol{S}_{52} & \boldsymbol{S}'_{52} & -\boldsymbol{S}_{53} & -\boldsymbol{S}'_{53} \\ & & \mathbf{0}_{4\times6} & & & \\ -\boldsymbol{S}_{51} & -\boldsymbol{S}'_{51} & -\boldsymbol{S}_{52} & -\boldsymbol{S}'_{52} & \mathbf{0} & \mathbf{0} \\ & & \mathbf{0}_{2\times6} & & & \end{bmatrix} \tag{C.6}$$

$$\mathbf{M}_{26}=\begin{bmatrix} \mathbf{0} & \mathbf{0} & \mathbf{0} & \mathbf{0} & \mathbf{0} & \mathbf{0} \\ \boldsymbol{S}_{61} & \boldsymbol{S}'_{61} & \mathbf{0} & \mathbf{0} & \boldsymbol{S}_{63} & \boldsymbol{S}'_{63} \\ \mathbf{0} & \mathbf{0} & \boldsymbol{S}_{62} & \boldsymbol{S}'_{62} & -\boldsymbol{S}_{63} & -\boldsymbol{S}'_{63} \\ & & \mathbf{0}_{5\times6} & & & \\ -\boldsymbol{S}_{61} & -\boldsymbol{S}'_{61} & -\boldsymbol{S}_{62} & -\boldsymbol{S}'_{62} & \mathbf{0} & \mathbf{0} \\ & & \mathbf{0}_{3\times6} & & & \end{bmatrix} \tag{C.7}$$

$$\mathbf{M}_{18}=\begin{bmatrix} & & \mathbf{0}_{2\times 6} & & & \\ \mathbf{0} & \mathbf{0} & \boldsymbol{S}_{82} & \boldsymbol{S}'_{82} & \boldsymbol{S}_{83} & \boldsymbol{S}'_{83} \\ & & \mathbf{0}_{4\times 6} & & & \\ \boldsymbol{S}_{81} & \boldsymbol{S}'_{81} & \mathbf{0} & \mathbf{0} & -\boldsymbol{S}_{83} & -\boldsymbol{S}'_{83} \\ -\boldsymbol{S}_{81} & -\boldsymbol{S}'_{81} & -\boldsymbol{S}_{82} & -\boldsymbol{S}'_{82} & \mathbf{0} & \mathbf{0} \\ & & \mathbf{0}_{3\times 6} & & & \end{bmatrix} \tag{C.8}$$

$$\mathbf{M}_{19}=\begin{bmatrix} & & & \mathbf{0}_{10\times 8} & & & & \\ \mathbf{0} & \mathbf{0} & \boldsymbol{S}_{92} & \boldsymbol{S}'_{92} & \boldsymbol{S}_{93} & \boldsymbol{S}'_{93} & \mathbf{0} & \mathbf{0} \\ \boldsymbol{S}_{91} & \boldsymbol{S}'_{91} & -\boldsymbol{S}_{92} & -\boldsymbol{S}'_{92} & \mathbf{0} & \mathbf{0} & \mathbf{0} & \mathbf{0} \end{bmatrix} \tag{C.9}$$

$$\mathbf{M}_{1-10}=\begin{bmatrix} & & & \mathbf{0}_{8\times 8} & & & & \\ \mathbf{0} & \mathbf{0} & \boldsymbol{S}_{10-2} & \boldsymbol{S}'_{10-2} & \boldsymbol{S}_{10-3} & \boldsymbol{S}'_{10-3} & \mathbf{0} & \mathbf{0} \\ \boldsymbol{S}_{10-1} & \boldsymbol{S}'_{10-1} & -\boldsymbol{S}_{10-2} & -\boldsymbol{S}'_{10-2} & \mathbf{0} & \mathbf{0} & \mathbf{0} & \mathbf{0} \\ & & & \mathbf{0}_{2\times 8} & & & & \end{bmatrix} \tag{C.10}$$

$$\mathbf{M}_{1-11}=\begin{bmatrix} & & & & \mathbf{0}_{6\times 8} & & & \\ \boldsymbol{S}_{11-1} & \boldsymbol{S}'_{11-1} & \mathbf{0} & \mathbf{0} & \mathbf{0} & \mathbf{0} & \boldsymbol{S}_{11-4} & \boldsymbol{S}'_{11-4} \\ \mathbf{0} & \mathbf{0} & \mathbf{0} & \mathbf{0} & \boldsymbol{S}_{11-3} & \boldsymbol{S}'_{11-3} & -\boldsymbol{S}_{11-4} & -\boldsymbol{S}'_{11-4} \\ & & & & \mathbf{0}_{4\times 8} & & & \end{bmatrix} \tag{C.11}$$

$$\mathbf{M}_{1-12}=\begin{bmatrix} & & & \mathbf{0}_{4\times 8} & & & & \\ \mathbf{0} & \mathbf{0} & \boldsymbol{S}_{12-2} & \boldsymbol{S}'_{12-2} & \boldsymbol{S}_{12-3} & \boldsymbol{S}'_{12-3} & \mathbf{0} & \mathbf{0} \\ \boldsymbol{S}_{12-1} & \boldsymbol{S}'_{12-1} & -\boldsymbol{S}_{12-2} & -\boldsymbol{S}'_{12-2} & \mathbf{0} & \mathbf{0} & \mathbf{0} & \mathbf{0} \\ & & & \mathbf{0}_{6\times 8} & & & & \end{bmatrix} \tag{C.12}$$

$$\mathbf{M}_{1-13}=\begin{bmatrix} \mathbf{0} & \mathbf{0} & \mathbf{0} & \mathbf{0} & \boldsymbol{S}_{13-3} & \boldsymbol{S}'_{13-3} & \boldsymbol{S}_{13-4} & \boldsymbol{S}'_{13-4} \\ \boldsymbol{S}_{13-1} & \boldsymbol{S}'_{13-1} & \mathbf{0} & \mathbf{0} & \mathbf{0} & \mathbf{0} & -\boldsymbol{S}_{13-4} & -\boldsymbol{S}'_{13-4} \\ -\boldsymbol{S}_{13-1} & -\boldsymbol{S}'_{13-1} & \boldsymbol{S}_{13-2} & \boldsymbol{S}'_{13-2} & \mathbf{0} & \mathbf{0} & \mathbf{0} & \mathbf{0} \\ \mathbf{0} & \mathbf{0} & -\boldsymbol{S}_{13-2} & -\boldsymbol{S}'_{13-2} & -\boldsymbol{S}_{13-3} & -\boldsymbol{S}'_{13-3} & \mathbf{0} & \mathbf{0} \\ & & & \mathbf{0}_{8\times 8} & & & & \end{bmatrix} \tag{C.13}$$

$$\mathbf{M}_{29}=\begin{bmatrix} & & & & \mathbf{0}_{6\times 8} & & & \\ \mathbf{0} & \mathbf{0} & \mathbf{0} & \mathbf{0} & -\boldsymbol{S}_{93} & -\boldsymbol{S}'_{93} & \boldsymbol{S}_{94} & \boldsymbol{S}'_{94} \\ -\boldsymbol{S}_{91} & -\boldsymbol{S}'_{91} & \mathbf{0} & \mathbf{0} & \mathbf{0} & \mathbf{0} & -\boldsymbol{S}_{94} & -\boldsymbol{S}'_{94} \\ & & & & \mathbf{0}_{4\times 8} & & & \end{bmatrix} \tag{C.14}$$

$$\mathbf{M}_{2-10}=\begin{bmatrix} & & & & \mathbf{0}_{4\times 8} & & & \\ \mathbf{0} & \mathbf{0} & \mathbf{0} & \mathbf{0} & -\boldsymbol{S}_{10-3} & -\boldsymbol{S}'_{10-3} & \boldsymbol{S}_{10-4} & \boldsymbol{S}'_{10-4} \\ -\boldsymbol{S}_{10-1} & -\boldsymbol{S}'_{10-1} & \mathbf{0} & \mathbf{0} & \mathbf{0} & \mathbf{0} & -\boldsymbol{S}_{10-4} & -\boldsymbol{S}'_{10-4} \\ & & & & \mathbf{0}_{6\times 8} & & & \end{bmatrix} \tag{C.15}$$

$$\mathbf{M}_{2-11}=\begin{bmatrix} & & & & \mathbf{0}_{2\times 8} & & & \\ -\boldsymbol{S}_{11-1} & -\boldsymbol{S}'_{11-1} & \boldsymbol{S}_{11-2} & \boldsymbol{S}'_{11-2} & \mathbf{0} & \mathbf{0} & \mathbf{0} & \mathbf{0} \\ \mathbf{0} & \mathbf{0} & -\boldsymbol{S}_{11-2} & -\boldsymbol{S}'_{11-2} & \boldsymbol{S}_{11-3} & \boldsymbol{S}'_{11-3} & \mathbf{0} & \mathbf{0} \\ & & & & \mathbf{0}_{8\times 8} & & & \end{bmatrix} \tag{C.16}$$

$$\mathbf{M}_{2-12} = \begin{bmatrix} \mathbf{0} & \mathbf{0} & \mathbf{0} & \mathbf{0} & -\boldsymbol{S}_{12-3} & -\boldsymbol{S}'_{12-3} & \boldsymbol{S}_{12-4} & \boldsymbol{S}'_{12-4} \\ -\boldsymbol{S}_{12-1} & -\boldsymbol{S}'_{12-1} & \mathbf{0} & \mathbf{0} & \mathbf{0} & \mathbf{0} & -\boldsymbol{S}_{12-4} & -\boldsymbol{S}'_{12-4} \\ & & & & \mathbf{0}_{10\times 8} & & & \end{bmatrix} \tag{C.17}$$

$$\mathbf{M}_{2-14} = \begin{bmatrix} & & & & \mathbf{0}_{8\times 8} & & & \\ \mathbf{0} & \mathbf{0} & \mathbf{0} & \mathbf{0} & \boldsymbol{S}_{14-3} & \boldsymbol{S}'_{14-3} & \boldsymbol{S}_{14-4} & \boldsymbol{S}'_{14-4} \\ \mathbf{0} & \mathbf{0} & \boldsymbol{S}_{14-2} & \boldsymbol{S}'_{14-2} & -\boldsymbol{S}_{14-3} & -\boldsymbol{S}'_{14-3} & \mathbf{0} & \mathbf{0} \\ \boldsymbol{S}_{14-1} & \boldsymbol{S}'_{14-1} & -\boldsymbol{S}_{14-2} & -\boldsymbol{S}'_{14-2} & \mathbf{0} & \mathbf{0} & \mathbf{0} & \mathbf{0} \\ -\boldsymbol{S}_{14-1} & -\boldsymbol{S}'_{14-1} & \mathbf{0} & \mathbf{0} & \mathbf{0} & \mathbf{0} & -\boldsymbol{S}_{14-4} & -\boldsymbol{S}'_{14-4} \end{bmatrix} \tag{C.18}$$

Appendix D.

$$\mathbf{R}_1 = \begin{bmatrix} \frac{\sqrt{6}}{6}\sin\theta_i - \frac{\sqrt{2}}{2}\cos\theta_i & -\frac{\sqrt{2}}{2}\cos\theta_i - \frac{\sqrt{6}}{6}\cos\theta_i & -\frac{\sqrt{3}}{3} \\ \frac{\sqrt{2}}{2}\cos\theta_i + \frac{\sqrt{6}}{6}\sin\theta_i & \frac{\sqrt{2}}{2}\sin\theta_i - \frac{\sqrt{6}}{6}\cos\theta_i & -\frac{\sqrt{3}}{3} \\ \frac{\sqrt{6}}{3}\sin\theta_i & -\frac{\sqrt{6}}{3}\cos\theta_i & \frac{\sqrt{3}}{3} \end{bmatrix} \tag{D.1}$$

$$\mathbf{R}_2 = \begin{bmatrix} \frac{\sqrt{6}}{3}\sin\theta_i & -\frac{\sqrt{6}}{3}\cos\theta_i & \frac{\sqrt{3}}{3} \\ \frac{\sqrt{6}}{6}\sin\theta_i - \frac{\sqrt{2}}{2}\cos\theta_i & -\frac{\sqrt{2}}{2}\sin\theta_i - \frac{\sqrt{6}}{6}\cos\theta_i & -\frac{\sqrt{3}}{3} \\ \frac{\sqrt{2}}{2}\cos\theta_i + \frac{\sqrt{6}}{6}\sin\theta_i & \frac{\sqrt{2}}{2}\sin\theta_i - \frac{\sqrt{6}}{6}\cos\theta_i & -\frac{\sqrt{3}}{3} \end{bmatrix} \tag{D.2}$$

$$\mathbf{R}_3 = \begin{bmatrix} -\frac{\sqrt{2}}{2}\cos\theta_i - \frac{\sqrt{6}}{6}\sin\theta_i & \frac{\sqrt{2}}{2}\sin\theta_i - \frac{\sqrt{6}}{6}\cos\theta_i & -\frac{\sqrt{3}}{3} \\ \frac{\sqrt{6}}{6}\sin\theta_i - \frac{\sqrt{2}}{2}\cos\theta_i & \frac{\sqrt{2}}{2}\sin\theta_i + \frac{\sqrt{6}}{6}\cos\theta_i & \frac{\sqrt{3}}{3} \\ \frac{\sqrt{6}}{3}\sin\theta_i & \frac{\sqrt{6}}{3}\cos\theta_i & -\frac{\sqrt{3}}{3} \end{bmatrix} \tag{D.3}$$

$$\mathbf{R}_4 = \begin{bmatrix} \frac{\sqrt{6}}{6}\sin\theta_i - \frac{\sqrt{2}}{2}\cos\theta_i & \frac{\sqrt{2}}{2}\sin\theta_i + \frac{\sqrt{6}}{6}\cos\theta_i & \frac{\sqrt{3}}{3} \\ -\frac{\sqrt{6}}{3}\sin\theta_i & -\frac{\sqrt{6}}{3}\cos\theta_i & \frac{\sqrt{3}}{3} \\ \frac{\sqrt{2}}{2}\cos\theta_i + \frac{\sqrt{6}}{6}\sin\theta_i & \frac{\sqrt{6}}{6}\cos\theta_i - \frac{\sqrt{2}}{2}\sin\theta_i & \frac{\sqrt{3}}{3} \end{bmatrix} \tag{D.4}$$

$$\mathbf{R}_5=\begin{bmatrix} \frac{\sqrt{2}}{2}\sin\theta_k+\frac{\sqrt{6}}{6}\cos\theta_k & \frac{\sqrt{6}}{6}\sin\theta_k-\frac{\sqrt{2}}{2}\cos\theta_k & -\frac{\sqrt{3}}{3} \\ -\frac{\sqrt{6}}{3}\cos\theta_k & -\frac{\sqrt{6}}{6}\sin\theta_k & -\frac{\sqrt{3}}{3} \\ \frac{\sqrt{6}}{6}\cos\theta_k-\frac{\sqrt{2}}{2}\sin\theta_k & \frac{\sqrt{2}}{2}\cos\theta_k+\frac{\sqrt{6}}{6}\sin\theta_k & -\frac{\sqrt{3}}{3} \end{bmatrix} \tag{D.5}$$

$$\mathbf{R}_6=\begin{bmatrix} -\frac{\sqrt{2}}{2}\sin\theta_k-\frac{\sqrt{6}}{6}\cos\theta_k & \frac{\sqrt{6}}{6}\sin\theta_k-\frac{\sqrt{2}}{2}\cos\theta_k & \frac{\sqrt{3}}{3} \\ \frac{\sqrt{6}}{6}\cos\theta_k-\frac{\sqrt{2}}{2}\sin\theta_k & -\frac{\sqrt{2}}{2}\cos\theta_k-\frac{\sqrt{6}}{6}\sin\theta_k & -\frac{\sqrt{3}}{3} \\ \frac{\sqrt{6}}{3}\cos\theta_k & -\frac{\sqrt{6}}{3}\sin\theta_k & \frac{\sqrt{3}}{3} \end{bmatrix} \tag{D.6}$$

$$\mathbf{R}_7=\begin{bmatrix} -\frac{\sqrt{6}}{3}\cos\theta_k & \frac{\sqrt{6}}{3}\sin\theta_k & -\frac{\sqrt{3}}{3} \\ -\frac{\sqrt{2}}{2}\sin\theta_k-\frac{\sqrt{6}}{6}\cos\theta_k & \frac{\sqrt{6}}{6}\sin\theta_k-\frac{\sqrt{2}}{2}\cos\theta_k & \frac{\sqrt{3}}{3} \\ \frac{\sqrt{2}}{2}\sin\theta_k-\frac{\sqrt{6}}{6}\cos\theta_k & \frac{\sqrt{2}}{2}\cos\theta_k+\frac{\sqrt{6}}{6}\sin\theta_k & \frac{\sqrt{3}}{3} \end{bmatrix} \tag{D.7}$$

$$\mathbf{R}_8=\begin{bmatrix} \frac{\sqrt{2}}{2}\sin\theta_k+\frac{\sqrt{6}}{6}\cos\theta_k & \frac{\sqrt{2}}{2}\cos\theta_k-\frac{\sqrt{6}}{6}\sin\theta_k & \frac{\sqrt{3}}{3} \\ -\frac{\sqrt{6}}{3}\cos\theta_k & \frac{\sqrt{6}}{3}\sin\theta_k & \frac{\sqrt{3}}{3} \\ \frac{\sqrt{2}}{2}\sin\theta_k-\frac{\sqrt{6}}{6}\cos\theta_k & \frac{\sqrt{2}}{2}\cos\theta_k+\frac{\sqrt{6}}{6}\sin\theta_k & -\frac{\sqrt{3}}{3} \end{bmatrix} \tag{D.8}$$

$$\boldsymbol{p}_1 = d_t'\begin{bmatrix} -\frac{\sqrt{3}}{3} & -\frac{\sqrt{3}}{3} & \frac{\sqrt{3}}{3} \end{bmatrix}^{\mathrm{T}} \tag{D.9}$$

$$\boldsymbol{p}_2 = d_t'\begin{bmatrix} \frac{\sqrt{3}}{3} & -\frac{\sqrt{3}}{3} & -\frac{\sqrt{3}}{3} \end{bmatrix}^{\mathrm{T}} \tag{D.10}$$

$$\boldsymbol{p}_3 = d_t'\begin{bmatrix} -\frac{\sqrt{3}}{3} & \frac{\sqrt{3}}{3} & -\frac{\sqrt{3}}{3} \end{bmatrix}^{\mathrm{T}} \tag{D.11}$$

$$\boldsymbol{p}_4 = d_t'\begin{bmatrix} \frac{\sqrt{3}}{3} & \frac{\sqrt{3}}{3} & \frac{\sqrt{3}}{3} \end{bmatrix}^{\mathrm{T}} \tag{D.12}$$

$$\boldsymbol{p}_5 = d_h\begin{bmatrix} -\frac{\sqrt{3}}{3} & -\frac{\sqrt{3}}{3} & -\frac{\sqrt{3}}{3} \end{bmatrix}^{\mathrm{T}} \tag{D.13}$$

$$\boldsymbol{p}_6 = d_h\begin{bmatrix} \frac{\sqrt{3}}{3} & -\frac{\sqrt{3}}{3} & \frac{\sqrt{3}}{3} \end{bmatrix}^{\mathrm{T}} \tag{D.14}$$

$$\boldsymbol{p}_7 = d_h \begin{bmatrix} -\frac{\sqrt{3}}{3} & \frac{\sqrt{3}}{3} & \frac{\sqrt{3}}{3} \end{bmatrix}^{\mathrm{T}} \tag{D.15}$$

$$\boldsymbol{p}_8 = d_h \begin{bmatrix} \frac{\sqrt{3}}{3} & \frac{\sqrt{3}}{3} & -\frac{\sqrt{3}}{3} \end{bmatrix}^{\mathrm{T}} \tag{D.16}$$

Appendix E.

$$\mathbf{M}_{11}=\begin{bmatrix} \mathbf{0} & \mathbf{0} & \mathbf{0} & \mathbf{0} & \mathbf{0} & \mathbf{0} \\ \mathbf{0} & \mathbf{0} & \boldsymbol{S}_{12} & \boldsymbol{S}'_{12} & \boldsymbol{S}_{13} & \boldsymbol{S}'_{13} \\ \boldsymbol{S}_{11} & \boldsymbol{S}'_{11} & \mathbf{0} & \mathbf{0} & -\boldsymbol{S}_{13} & -\boldsymbol{S}'_{13} \\ -\boldsymbol{S}_{11} & -\boldsymbol{S}'_{11} & -\boldsymbol{S}_{12} & -\boldsymbol{S}'_{12} & \mathbf{0} & \mathbf{0} \\ \multicolumn{6}{c}{\mathbf{0}_{5\times 6}} \end{bmatrix} \tag{E.1}$$

$$\mathbf{M}_{12}=\begin{bmatrix} \multicolumn{6}{c}{\mathbf{0}_{8\times 6}} \\ \boldsymbol{S}_{21} & \boldsymbol{S}'_{21} & \mathbf{0} & \mathbf{0} & \boldsymbol{S}_{23} & \boldsymbol{S}'_{23} \end{bmatrix} \tag{E.2}$$

$$\mathbf{M}_{14}=\begin{bmatrix} \multicolumn{6}{c}{\mathbf{0}_{5\times 6}} \\ \boldsymbol{S}_{41} & \boldsymbol{S}'_{41} & \mathbf{0} & \mathbf{0} & \boldsymbol{S}_{43} & \boldsymbol{S}'_{43} \\ \mathbf{0} & \mathbf{0} & \mathbf{0} & \mathbf{0} & \mathbf{0} & \mathbf{0} \\ -\boldsymbol{S}_{41} & -\boldsymbol{S}'_{41} & \boldsymbol{S}_{42} & \boldsymbol{S}'_{42} & \mathbf{0} & \mathbf{0} \\ \mathbf{0} & \mathbf{0} & \mathbf{0} & \mathbf{0} & \mathbf{0} & \mathbf{0} \end{bmatrix} \tag{E.3}$$

$$\mathbf{M}_{22}=\begin{bmatrix} \mathbf{0} & \mathbf{0} & \boldsymbol{S}_{22} & \boldsymbol{S}'_{22} & -\boldsymbol{S}_{23} & -\boldsymbol{S}'_{23} \\ \multicolumn{6}{c}{\mathbf{0}_{3\times 6}} \\ -\boldsymbol{S}_{21} & -\boldsymbol{S}'_{21} & -\boldsymbol{S}_{22} & -\boldsymbol{S}'_{22} & \mathbf{0} & \mathbf{0} \\ \multicolumn{6}{c}{\mathbf{0}_{4\times 6}} \end{bmatrix} \tag{E.4}$$

$$\mathbf{M}_{23}=\begin{bmatrix} \multicolumn{6}{c}{\mathbf{0}_{6\times 6}} \\ \mathbf{0} & \mathbf{0} & \boldsymbol{S}_{32} & \boldsymbol{S}'_{32} & \boldsymbol{S}_{33} & \boldsymbol{S}'_{33} \\ \boldsymbol{S}_{31} & \boldsymbol{S}'_{31} & -\boldsymbol{S}_{32} & -\boldsymbol{S}'_{32} & \mathbf{0} & \mathbf{0} \\ -\boldsymbol{S}_{31} & -\boldsymbol{S}'_{31} & \mathbf{0} & \mathbf{0} & -\boldsymbol{S}_{33} & -\boldsymbol{S}'_{33} \end{bmatrix} \tag{E.5}$$

$$\mathbf{M}_{24}=\begin{bmatrix} \multicolumn{6}{c}{\mathbf{0}_{2\times 6}} \\ \mathbf{0} & \mathbf{0} & -\boldsymbol{S}_{42} & -\boldsymbol{S}'_{42} & -\boldsymbol{S}_{43} & -\boldsymbol{S}'_{43} \\ \multicolumn{6}{c}{\mathbf{0}_{6\times 6}} \end{bmatrix} \tag{E.6}$$

$$\mathbf{M}_{15}=\begin{bmatrix} \boldsymbol{S}_{51} & \boldsymbol{S}'_{51} & \boldsymbol{S}_{52} & \boldsymbol{S}'_{52} & \mathbf{0} & \mathbf{0} & \mathbf{0} & \mathbf{0} & \mathbf{0} & \mathbf{0} & \mathbf{0} & \mathbf{0} \\ \mathbf{0} & \mathbf{0} & \mathbf{0} & \mathbf{0} & \mathbf{0} & \mathbf{0} & \mathbf{0} & \mathbf{0} & \mathbf{0} & \mathbf{0} & \mathbf{0} & \mathbf{0} \\ -\boldsymbol{S}_{51} & -\boldsymbol{S}'_{51} & \mathbf{0} & \mathbf{0} & \mathbf{0} & \mathbf{0} & \mathbf{0} & \mathbf{0} & \mathbf{0} & \mathbf{0} & \boldsymbol{S}_{56} & \boldsymbol{S}'_{56} \\ \multicolumn{12}{c}{\mathbf{0}_{3\times 12}} \\ \mathbf{0} & \mathbf{0} & \mathbf{0} & \mathbf{0} & \mathbf{0} & \mathbf{0} & \mathbf{0} & \mathbf{0} & \boldsymbol{S}_{55} & \boldsymbol{S}'_{55} & -\boldsymbol{S}_{56} & -\boldsymbol{S}'_{56} \\ \mathbf{0} & \mathbf{0} & \mathbf{0} & \mathbf{0} & \mathbf{0} & \mathbf{0} & \mathbf{0} & \mathbf{0} & \mathbf{0} & \mathbf{0} & \mathbf{0} & \mathbf{0} \\ \mathbf{0} & \mathbf{0} & \mathbf{0} & \mathbf{0} & \mathbf{0} & \mathbf{0} & \boldsymbol{S}_{54} & \boldsymbol{S}'_{54} & -\boldsymbol{S}_{55} & -\boldsymbol{S}'_{55} & \mathbf{0} & \mathbf{0} \end{bmatrix} \tag{E.7}$$

$$\mathbf{M}_{16}=\begin{bmatrix} \multicolumn{12}{c}{\mathbf{0}_{3\times 12}} \\ \boldsymbol{S}_{61} & \boldsymbol{S}'_{61} & \mathbf{0} & \mathbf{0} & \mathbf{0} & \mathbf{0} & \mathbf{0} & \mathbf{0} & \mathbf{0} & \mathbf{0} & \boldsymbol{S}_{66} & \boldsymbol{S}'_{66} \\ \mathbf{0} & \mathbf{0} & \mathbf{0} & \mathbf{0} & \mathbf{0} & \mathbf{0} & \mathbf{0} & \mathbf{0} & \boldsymbol{S}_{65} & \boldsymbol{S}'_{65} & -\boldsymbol{S}_{66} & -\boldsymbol{S}'_{66} \\ \mathbf{0} & \mathbf{0} & \mathbf{0} & \mathbf{0} & \mathbf{0} & \mathbf{0} & \mathbf{0} & \mathbf{0} & \mathbf{0} & \mathbf{0} & \mathbf{0} & \mathbf{0} \\ -\boldsymbol{S}_{61} & -\boldsymbol{S}'_{61} & \boldsymbol{S}_{62} & \boldsymbol{S}'_{62} & \mathbf{0} & \mathbf{0} & \mathbf{0} & \mathbf{0} & \mathbf{0} & \mathbf{0} & \mathbf{0} & \mathbf{0} \\ \mathbf{0} & \mathbf{0} & \mathbf{0} & \mathbf{0} & \mathbf{0} & \mathbf{0} & \boldsymbol{S}_{64} & \boldsymbol{S}'_{64} & -\boldsymbol{S}_{65} & -\boldsymbol{S}'_{65} & \mathbf{0} & \mathbf{0} \\ \mathbf{0} & \mathbf{0} & \mathbf{0} & \mathbf{0} & \mathbf{0} & \mathbf{0} & \mathbf{0} & \mathbf{0} & \mathbf{0} & \mathbf{0} & \mathbf{0} & \mathbf{0} \end{bmatrix} \tag{E.8}$$

$$\mathbf{M}_{17}=\begin{bmatrix} \mathbf{0} & \mathbf{0} & \mathbf{0} & \mathbf{0} & \mathbf{0} & \mathbf{0} & \mathbf{0} & \mathbf{0} & \boldsymbol{S}_{75} & \boldsymbol{S}'_{75} & \boldsymbol{S}_{76} & \boldsymbol{S}'_{76} \\ \boldsymbol{S}_{71} & \boldsymbol{S}'_{71} & \mathbf{0} & \mathbf{0} & \mathbf{0} & \mathbf{0} & \mathbf{0} & \mathbf{0} & \mathbf{0} & \mathbf{0} & -\boldsymbol{S}_{76} & -\boldsymbol{S}'_{76} \\ \multicolumn{12}{c}{\mathbf{0}_{2\times 12}} \\ -\boldsymbol{S}_{71} & -\boldsymbol{S}'_{71} & \boldsymbol{S}_{72} & \boldsymbol{S}'_{72} & \mathbf{0} & \mathbf{0} & \mathbf{0} & \mathbf{0} & \mathbf{0} & \mathbf{0} & \mathbf{0} & \mathbf{0} \\ \mathbf{0} & \mathbf{0} & -\boldsymbol{S}_{72} & -\boldsymbol{S}'_{72} & \boldsymbol{S}_{73} & \boldsymbol{S}'_{73} & \mathbf{0} & \mathbf{0} & \mathbf{0} & \mathbf{0} & \mathbf{0} & \mathbf{0} \\ \multicolumn{12}{c}{\mathbf{0}_{3\times 12}} \end{bmatrix} \tag{E.9}$$

$$\mathbf{M}_{25}=\begin{bmatrix} \multicolumn{12}{c}{\mathbf{0}_{5\times 12}} \\ \mathbf{0} & \mathbf{0} & \mathbf{0} & \mathbf{0} & \boldsymbol{S}_{53} & \boldsymbol{S}'_{53} & -\boldsymbol{S}_{54} & -\boldsymbol{S}'_{54} & \mathbf{0} & \mathbf{0} & \mathbf{0} & \mathbf{0} \\ \multicolumn{12}{c}{\mathbf{0}_{2\times 12}} \\ \mathbf{0} & \mathbf{0} & -\boldsymbol{S}_{52} & -\boldsymbol{S}'_{52} & -\boldsymbol{S}_{53} & \boldsymbol{S}'_{53} & \mathbf{0} & \mathbf{0} & \mathbf{0} & \mathbf{0} & \mathbf{0} & \mathbf{0} \end{bmatrix} \tag{E.10}$$

$$\mathbf{M}_{26}=\begin{bmatrix} \mathbf{0} & \mathbf{0} & -\boldsymbol{S}_{62} & -\boldsymbol{S}'_{62} & \boldsymbol{S}_{63} & \boldsymbol{S}'_{63} & \mathbf{0} & \mathbf{0} & \mathbf{0} & \mathbf{0} & \mathbf{0} & \mathbf{0} \\ \mathbf{0} & \mathbf{0} & \mathbf{0} & \mathbf{0} & -\boldsymbol{S}_{63} & -\boldsymbol{S}'_{63} & -\boldsymbol{S}_{64} & -\boldsymbol{S}'_{64} & \mathbf{0} & \mathbf{0} & \mathbf{0} & \mathbf{0} \\ \multicolumn{12}{c}{\mathbf{0}_{7\times 12}} \end{bmatrix} \tag{E.11}$$

$$\mathbf{M}_{27}=\begin{bmatrix} \multicolumn{12}{c}{\mathbf{0}_{3\times 12}} \\ \mathbf{0} & \mathbf{0} & \mathbf{0} & \mathbf{0} & -\boldsymbol{S}_{73} & -\boldsymbol{S}'_{73} & \boldsymbol{S}_{74} & \boldsymbol{S}'_{74} & \mathbf{0} & \mathbf{0} & \mathbf{0} & \mathbf{0} \\ \multicolumn{12}{c}{\mathbf{0}_{3\times 12}} \\ \mathbf{0} & \mathbf{0} & \mathbf{0} & \mathbf{0} & \mathbf{0} & \mathbf{0} & -\boldsymbol{S}_{74} & -\boldsymbol{S}'_{74} & -\boldsymbol{S}_{75} & -\boldsymbol{S}'_{75} & \mathbf{0} & \mathbf{0} \\ \mathbf{0} & \mathbf{0} & \mathbf{0} & \mathbf{0} & \mathbf{0} & \mathbf{0} & \mathbf{0} & \mathbf{0} & \mathbf{0} & \mathbf{0} & \mathbf{0} & \mathbf{0} \end{bmatrix} \tag{E.12}$$

$$\mathbf{M}_{28}=\begin{bmatrix} \mathbf{0} & \mathbf{0} & \mathbf{0} & \mathbf{0} & \mathbf{0} & \mathbf{0} & \mathbf{0} & \mathbf{0} & \mathbf{0} & \mathbf{0} & \mathbf{0} & \mathbf{0} \\ \boldsymbol{S}_{81} & \boldsymbol{S}'_{81} & \boldsymbol{S}_{82} & \boldsymbol{S}'_{82} & \mathbf{0} & \mathbf{0} & \mathbf{0} & \mathbf{0} & \mathbf{0} & \mathbf{0} & \mathbf{0} & \mathbf{0} \\ -\boldsymbol{S}_{81} & -\boldsymbol{S}'_{81} & \mathbf{0} & \mathbf{0} & \mathbf{0} & \mathbf{0} & \mathbf{0} & \mathbf{0} & \mathbf{0} & \mathbf{0} & \boldsymbol{S}_{86} & \boldsymbol{S}'_{86} \\ \mathbf{0} & \mathbf{0} & \mathbf{0} & \mathbf{0} & \mathbf{0} & \mathbf{0} & \mathbf{0} & \mathbf{0} & \boldsymbol{S}_{85} & \boldsymbol{S}'_{85} & -\boldsymbol{S}_{86} & -\boldsymbol{S}'_{86} \\ \mathbf{0} & \mathbf{0} & -\boldsymbol{S}_{82} & -\boldsymbol{S}'_{82} & \boldsymbol{S}_{83} & \boldsymbol{S}'_{83} & \mathbf{0} & \mathbf{0} & \mathbf{0} & \mathbf{0} & \mathbf{0} & \mathbf{0} \\ \mathbf{0} & \mathbf{0} & \mathbf{0} & \mathbf{0} & -\boldsymbol{S}_{83} & -\boldsymbol{S}'_{83} & \boldsymbol{S}_{84} & \boldsymbol{S}'_{84} & \mathbf{0} & \mathbf{0} & \mathbf{0} & \mathbf{0} \\ \mathbf{0} & \mathbf{0} & \mathbf{0} & \mathbf{0} & \mathbf{0} & \mathbf{0} & -\boldsymbol{S}_{84} & -\boldsymbol{S}'_{84} & -\boldsymbol{S}_{85} & -\boldsymbol{S}'_{85} & \mathbf{0} & \mathbf{0} \\ \multicolumn{12}{c}{\mathbf{0}_{2\times 12}} \end{bmatrix} \tag{E.13}$$